Crosstalk between AML and stromal cells triggers acetate secretion through the metabolic rewiring of stromal cells

Nuria Vilaplana-Lopera[1], Ruba Almaghrabi[1*], Grigorios Papatzikas[1*], Vincent Cuminetti[2*], Mark Jeeves[1], Elena González[1], Alan Cunningham[3], Ayşegül Erdem[3], Frank Schnuetgen[4,5,6], Manoj Raghavan[1,7], Sandeep Potluri[1,7], Jean-Baptiste Cazier[1], Jan Jacob Schuringa[3], Michelle AC Reed[1], Lorena Arranz[2], Ulrich L Günther[1,8†] and Paloma Garcia[1,9†],

[1] Institute of Cancer and Genomic Sciences, University of Birmingham, Birmingham B15 2TT, United Kingdom
[2] Stem Cells, Ageing and Cancer Research Group, Department of Medical Biology, Faculty of Health Sciences, UiT – The Arctic University of Norway, 9019 Tromsø, Norway
[3] Department of Experimental Hematology, University Medical Center Groningen, University of Groningen, Hanzeplein 1, 9700 RB, Groningen, The Netherlands.
[4] Department of Medicine, Hematology/Oncology, University Hospital Frankfurt, Goethe-University, 60590 Frankfurt, Germany.
[5] Frankfurt Cancer Institute, Goethe-University Frankfurt, 60596 Frankfurt, Germany.
[6] German Cancer Consortium (DKTK), partner site Frankfurt/Mainz, and German Cancer Research Center (DKFZ), Heidelberg, Germany
[7] Centre for Clinical Haematology, University Hospitals Birmingham NHS Foundation Trust, Queen Elizabeth Hospital, Queen Elizabeth Medical Centre, Birmingham, United Kingdom.
[8] Institute of Chemistry and Metabolomics, University of Lübeck, 23562 Lübeck, Germany
[9] Corresponding author
[*] These authors contributed equally
[†] These two authors are co-senior authors.

Acute myeloid leukaemia (AML) cells interact and modulate components of their surrounding microenvironment into their own benefit. Stromal cells have been shown to support AML survival and progression through various mechanisms. Nonetheless, it is unclear whether AML cells could establish beneficial metabolic interactions with stromal cells. Here, we identify a novel metabolic crosstalk between AML and stromal cells where AML cells prompt stromal cells to secrete acetate for their own consumption to feed the tricarboxylic acid cycle (TCA). By performing transcriptome analysis, tracer-based metabolic NMR analysis and ROS measurements, we observe that stromal cells present a higher rate of glycolysis. We also find that acetate in stromal cells is derived from pyruvate via chemical conversion under the influence of reactive oxygen species (ROS) following ROS transfer from AML to stromal cells via gap junctions. Overall, we present a unique metabolic communication between AML and stromal cells that could potentially be exploited for adjuvant therapy.

Keywords: Leukaemic niche, acetate, AML, tracer-based NMR, metabolic crosstalk, ROS, acetate metabolism, gap junctions

Introduction

Acute myeloid leukaemia (AML) is a heterogeneous clonal disease characterised by a rapid proliferation of aberrant immature myeloid cells that accumulate in the bone marrow, and eventually in the blood and other organs, severely impairing normal haematopoiesis. AML cells show a highly adaptive metabolism that allows them to efficiently use a variety of nutrients to obtain energy and generate biomass (reviewed in [1]). This high metabolic plasticity confers AML cells a strong advantage against normal haematopoietic cells and has been related to AML aggressiveness. Although the metabolism in AML cells has been broadly investigated [1], fewer studies have focused on identifying metabolic alterations related to the interaction between AML and niche cells. For instance, AML cells are known to interact and modulate niche components for their own support by secreting soluble factors [2-6], via exosomes [7-9] or by establishing direct interactions, mediated by gap junctions [10] or tunnelling nanotubes [11]. These interactions with components of the niche provide AML cells with survival cues, chemoresistance and increased relapse in AML patients [2,4,7,10,12-14]. Furthermore, it has been reported that adipocytes in the niche secrete fatty acids, which are metabolised by AML cells through β-oxidation to obtain energy, protecting AML cells from apoptosis and ROS [15,16].

As a consequence of their highly proliferative demand, leukaemic stem cells (LSCs) [17-20] and, particularly, chemotherapy-resistant AML cells [21] present abnormally high levels of reactive oxygen species (ROS) [22,23]. How AML cells cope with high ROS levels has been intriguing and recent reports are shedding some light on whether the microenvironment plays a role in the redox metabolism of AML cells. For instance, it was reported that Nestin^{+} bone marrow mesenchymal stem cells (BMSCs) support AML progression by increasing the bioenergetic capacity of AML cells and providing them with glutathione (GSH)-mediated antioxidant defence to balance the excess ROS [14]. Similarly, a recent study showed that co-culturing BMSCs with AML cells leads to a decrease in AML ROS levels due to an activation of the antioxidant enzyme GPx-3 in AML cells [24].

Our work provides new insight into the metabolic and redox crosstalk between AML and stromal cells, revealing a new metabolic interaction between AML and stromal cells. By combining transcriptomic and nuclear magnetic resonance (NMR) data, our results demonstrate that stromal cell metabolism is rewired in co-culture giving higher glycolysis and pyruvate decarboxylation, leading to acetate secretion. Our results also show that AML cells are able to transfer ROS to stromal cells by direct interaction through gap junctions and that these ROS can be used by stromal cells to generate and secrete acetate, which is utilised by AML cells as a biofuel by metabolising it via the

72 TCA cycle. Targeting ROS transfer via modulation of gap junctions to suppress the antioxidant
73 protection provided by stromal cells could serve as an adjuvant therapy to eradicate AML.

Results

Co-culturing AML and stromal cells in direct contact triggers acetate secretion by stromal cells

We first sought to determine whether interactions between AML and stromal cells in co-culture would result in differences in the consumption or production of extracellular metabolites. For this purpose, three AML cell lines (SKM-1, Kasumi-1 and HL-60) were cultured separately and in co-culture with MS-5, a stromal cell line capable of maintaining hematopoiesis [25], and the metabolic composition of the extracellular medium was analysed by ^{1}H-NMR and compared at different time points. The most striking difference found in co-culture compared to cells cultured separately was an increased secretion of acetate, which was common for the three cell lines used (Fig. 1a,b). Moreover, only stromal cells secreted acetate to a lower extent when cultured alone whereas AML cells did not secrete any acetate when cultured alone. Altogether, these findings suggest that acetate secretion is indeed a result of a direct interaction between AML and stromal cells. In addition, the observation that only stromal cells secrete acetate under these conditions suggests that stromal cells could be responsible for the increased acetate secretion found in co-culture.

Moreover, we examined the levels of other common extracellular metabolites, including glucose, lactate, glutamate and glutamine. As shown in Supplementary Fig. 1a higher consumption of glucose along with a higher secretion of lactate was observed in AML and stromal cells in co-culture compared to single cultures, suggesting a higher glycolytic flux in co-culture. However, the levels of glucose consumption and lactate production in co-culture were similar to the sum of the glucose consumption and lactate production levels of the AML and stromal cells in single cultures, suggesting that the overall increase in glycolysis in co-culture was just a result of culturing both cell types together. Additionally, we observed no variation in glutamate and glutamine levels suggesting that these metabolites are not involved in interactions that result from co-culture and are utilised depending on their availability.

The metabolic differences found in co-culture, could be due to altered proliferation under these conditions. To determine whether this was the case, a CFSE-based proliferation assay was performed in which AML cells and not stromal cells were stained and their growth was compared when cultured separately vs in co-culture. Over 48 hours, none of the AML cell lines tested presented differences in their proliferation rates (Supplementary Fig. 2a), thus confirming that the metabolic changes found in co-culture were caused by a mechanism independent from changes in proliferation.

Next, we aimed to determine whether cell-to-cell contact could play a role in the increased acetate secretion found in co-culture. For this we co-cultured AML and stromal cells separated by a permeable membrane, allowing cells to share the extracellular medium but impeding cell-to-cell

107 contact. Co-culturing cells using a permeable membrane blocked the increase in acetate secretion
108 observed under direct contact conditions (Fig. 1c). In fact, cells in co-culture presented lower levels
109 of acetate than MS-5 cells cultured alone revealing that direct cell-to-cell contact is required for
110 acetate secretion in co-culture.

111 To examine whether increased acetate secretion is specific for the interaction of AML cells with
112 stromal cells, we co-cultured AML cells with the cervical cancer cell line HeLa and compared the
113 levels of acetate of each cell type cultured alone. We found that there was no acetate secretion in
114 co-culture, also not by HeLa and AML cells cultured alone (Supplementary Fig. 2b), suggesting that
115 increased acetate secretion could be specific for the AML-stromal interaction.

116 Considering that our previous data seemed to indicate that MS-5 cells were responsible for acetate
117 secretion when co-cultured with AML cell lines, we decided to investigate how the levels of
118 extracellular acetate would vary after separating cells from co-culture. The three AML cell lines were
119 co-cultured for 24h with MS-5 cells prior to separation and were subsequently cultured in the same
120 spent media. Extracellular acetate levels in previously co-cultured MS-5 cells followed a similar trend
121 as before separation, suggesting that it is most likely that MS-5 cells are responsible for the
122 increased acetate secretion found in co-culture (Fig. 1d). Moreover, AML cells did not follow this
123 trend as they either maintained the levels of acetate seen prior to separating the cells (Kasumi-1 and
124 HL-60) or presented only a moderate increase (SKM-1) after being separated from co-culture.

125 We further investigated whether increased acetate secretion could take place in co-cultures, using
126 primary AML cells from patients, and whether acetate secretion in co-culture could be specific for
127 AML cells. To address this question, we isolated the $CD34^+$ population of four primary AML patient
128 samples, and three independent healthy donors, cultured them alone vs in co-culture with MS-5
129 cells, and analysed the composition of the extracellular medium at different time points. We found
130 that three out of four primary AML samples presented higher levels of acetate when co-cultured
131 with MS-5 cells compared to both MS-5 and AML cells cultured alone (Fig. 1e). Contrary, none of the
132 healthy donor samples showed an increased acetate secretion in co-culture suggesting that acetate
133 secretion is specific for AML cells in co-culture (Fig. 1f).

134 Moreover, we sought to determine whether in an experimental *in vivo* setting, increased acetate
135 production would be observed. For this, acetate levels were analysed in the bone marrow
136 extracellular fluid (BMEF) of mice transplanted either with MLL-AF9 leukaemic cells or with healthy
137 wild type hematopoietic cells. These experiments revealed higher amounts of acetate in the BMEF of
138 mice suffering from leukaemia compared to controls (Fig. 1g).

139

1

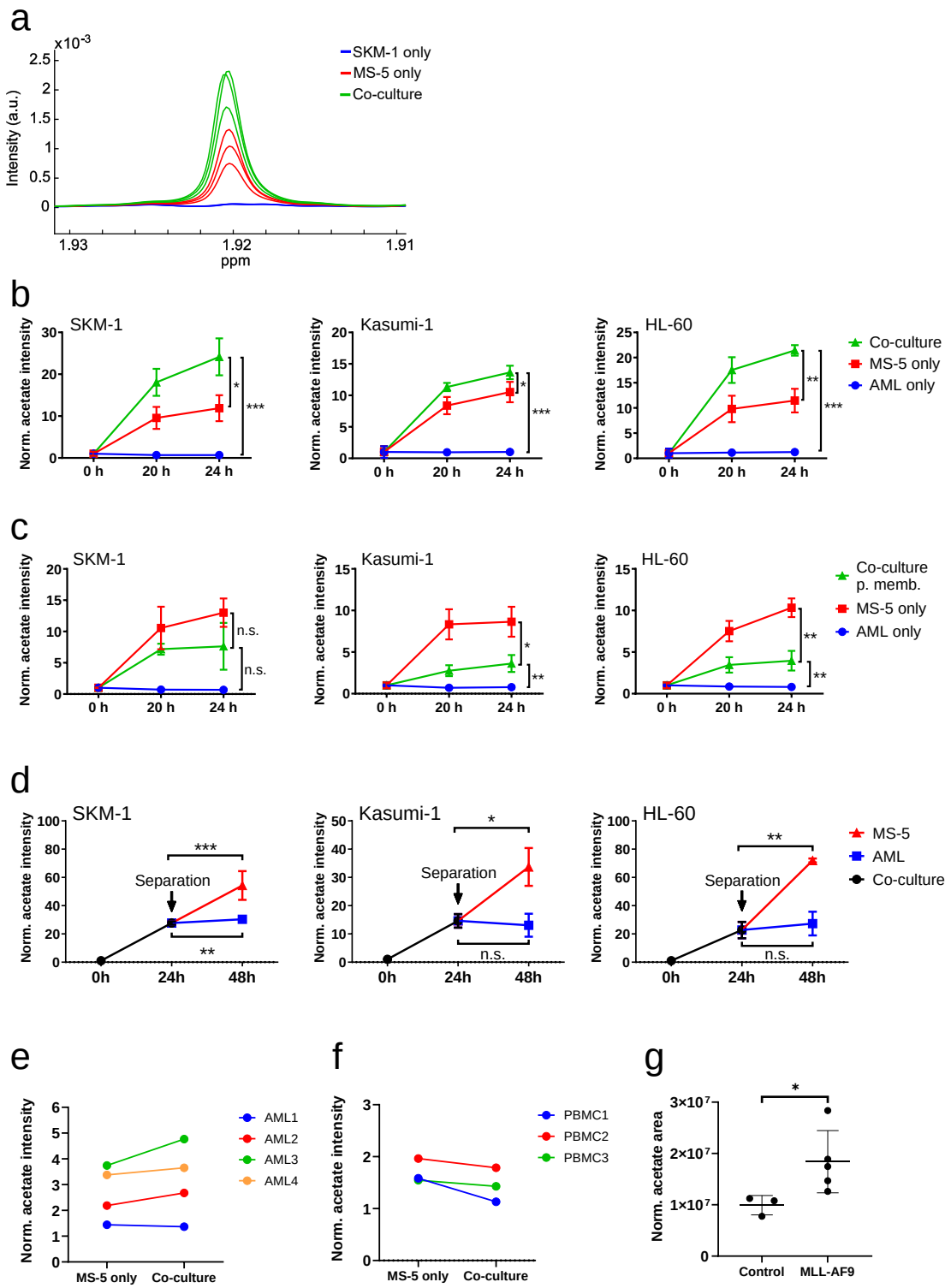
a
x10-3
Intensity (a.u.)
SKM-1 only
MS-5 only
Co-culture
ppm
b
SKM-1
Kasumi-1
HL-60
Norm. acetate intensity
0 h
20 h
24 h
Co-culture
MS-5 only
AML only
c
Co-culture p. memb.
n.s.
d
Separation
0h
24h
48h
MS-5
AML
e
AML1
AML2
AML3
AML4
MS-5 only
Co-culture
f
PBMC1
PBMC2
PBMC3
g
Norm. acetate area
Control
MLL-AF9

140

141

142 **Fig 1. Acetate secretion by stromal cells increases in AML-stroma co-cultures of several**
143 **AML cell lines and primary AML cells in direct contact. a,** Section of ^{1}H-NMR spectra,
144 corresponding to the methyl group of acetate, from extracellular medium samples of SKM-1 cells
145 cultured alone (blue), MS-5 cells cultured alone (red) and SKM-1 and MS-5 cells in co-culture (green)
146 after 24 hours. **b,** Extracellular acetate levels in AML cell lines (SKM-1, Kasumi-1 and HL-60) cultured
147 alone (blue), MS-5 cells cultured alone (red) and AML and MS-5 cells in co-culture in direct contact
148 (green) at 0, 20 and 24 hours of incubation. Each point represents the mean of n=3 independent
149 experiments and error bars represent standard deviations. **c,** Extracellular acetate levels in AML cell
150 lines cultured alone (blue), MS-5 cells cultured alone (red) and AML and MS-5 cells in co-culture
151 separated by a 0.4 µm permeable membrane (green) at 0, 20 and 24 hours of incubation. Each point
152 represents the mean of n=3 independent experiments and error bars represent standard deviations.
153 **d,** Extracellular acetate levels in AML cell lines and MS-5 cells in co-culture (black) for 24 hours and
154 after being separated and cultured alone in the same medium until 48 hours (blue for AML and red
155 for MS-5). Each point represents the mean of n=3 independent experiments and error bars
156 represent standard deviations.

157 For **b**, **c, d** and **g** unpaired Student's t-tests were applied for each condition (black brackets) and p-
158 values are represented by n.s. for not significant * for p-value<0.05, ** for p-value<0.01 and *** for
159 p-value<0.001.

160 **e,** Extracellular acetate levels in MS-5 cells cultured alone (black) and primary patient-derived AML
161 cells co-cultured with MS-5 cells (grey) at 48h. Each set of points represents an independent
162 experiment (n=4). **f,** Extracellular acetate levels in MS-5 cells cultured alone (black) and healthy
163 donor-derived peripheral blood mononuclear $CD34^{+}$ (PBMC) cells co-cultured with MS-5 cells (grey)
164 at 48h. Each set of points represents an independent experiment (n=3). **g**, Acetate levels in bone
165 marrow extracellular fluid of C57BL6/J mice 6 months after transplantation with bone marrow
166 nucleated cells isolated from control or MLL-AF9 transgenic mice. A Mann-Whitney test was applied
167 (black bracket) and p-value was represented as * for p-value<0.05 (p=0.0357).

168

169 **AML cells consume and use acetate secreted by stromal cells to feed the TCA cycle**

170 Following the finding that stromal cells are responsible for acetate secretion in co-culture, we
171 decided to determine whether AML cells might be able to metabolise the secreted acetate. We first
172 sought to define the concentration of secreted acetate in the extracellular medium in co-culture. For
173 this, we compared a sample of extracellular medium from a co-culture of SKM-1 and MS-5 cells after
174 24 hours to a calibration curve (Supplementary Fig. 2c) which allowed us to determine that the
175 concentration of acetate in co-culture, which was approximately of 3 mM. We then investigated
176 whether SKM-1 cells can consume acetate both in physiological and co-culture concentrations. In
177 both cases SKM-1 cells consumed acetate after 48 hours, and in physiological conditions also after
178 24 hours (Fig. 2a).

179 We used a tracer-based approach using [2-^{13}C]acetate to assess whether SKM-1 or MS-5 cells can
180 utilise acetate (Fig. 2b,c and Supplementary Fig. 3a). Both cell types import ^{13}C labelled acetate as
181 observed in NMR spectra (Fig. 2c). However, only SKM-1 cells showed ^{13}C label incorporation in
182 several TCA cycle related metabolites, including aspartate, citrate, glutamate, 2-oxoglutarate,
183 glutathione and proline, as well as in acetylcarnitine. Acetylcarnitine is known to be produced by
184 cells when large amounts of acetyl-CoA are present in the mitochondria [26,27], which could be in line
185 with this experiment in which a 4 mM concentration of [2-^{13}C]acetate was used. Overall, this data
186 suggests that acetate in co-culture could be utilised by SKM-1 cells but not by MS-5 cells.

187 In order to determine whether AML cells can import and metabolise the secreted acetate in co-
188 culture, we co-cultured AML and MS-5 cells for 24 hours, we then added [2-^{13}C]acetate to the spent
189 extracellular medium and cultured cells for 8 hours before analysing the intracellular metabolites in
190 each cell type (Fig. 2d). We found that only AML cells presented ^{13}C labelling in intracellular
191 metabolites (Fig. 2e, Supplementary Fig. 3b). Moreover, the metabolisation pattern for all AML cells
192 was similar to that observed for SKM-1 cells alone (Fig. 2c), where label was incorporated into TCA
193 cycle-related metabolites. Overall, these results revealed that AML cells uptake and utilise the
194 acetate secreted by stromal cells in co-culture as a substrate to feed into the TCA cycle.

195

2

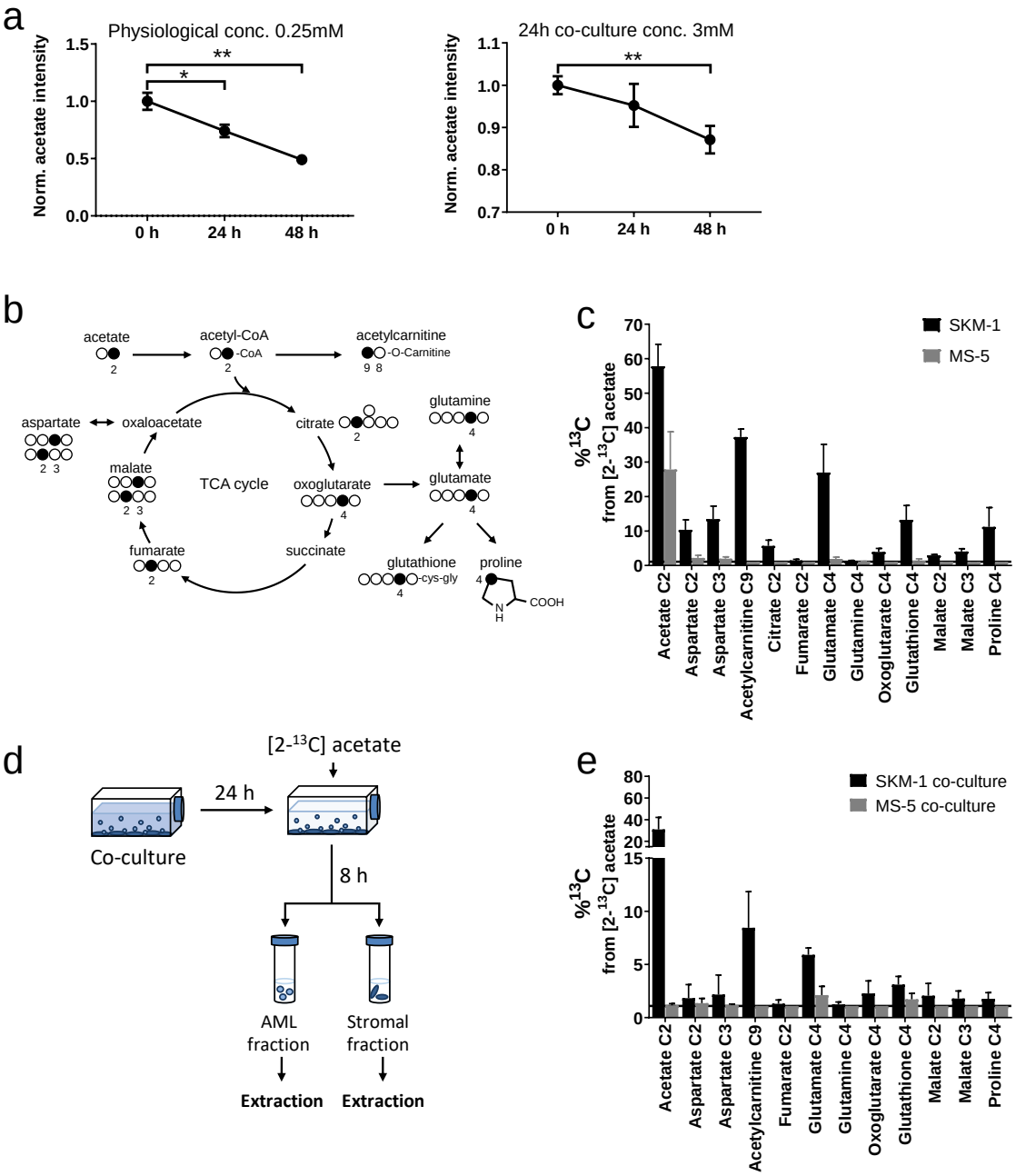
a
Physiological conc. 0.25mM
Norm. acetate intensity
1.5
1.0
0.5
0.0
**
*
0 h
24 h
48 h
24h co-culture conc. 3mM
Norm. acetate intensity
1.1
1.0
0.9
0.8
0.7
**
0 h
24 h
48 h
b
acetate
acetyl-CoA
-CoA
acetylcarnitine
-O-Carnitine
aspartate
oxaloacetate
citrate
glutamine
malate
TCA cycle
oxoglutarate
glutamate
fumarate
succinate
glutathione
-cys-gly
proline
COOH
c
SKM-1
MS-5
%13C
from [2-13C] acetate
Acetate C2
Aspartate C2
Aspartate C3
Acetylcarnitine C9
Citrate C2
Fumarate C2
Glutamate C4
Glutamine C4
Oxoglutarate C4
Glutathione C4
Malate C2
Malate C3
Proline C4
d
[2-13C] acetate
24 h
Co-culture
8 h
AML fraction
Stromal fraction
Extraction
Extraction
e
SKM-1 co-culture
MS-5 co-culture
%13C
from [2-13C] acetate
Acetate C2
Aspartate C2
Aspartate C3
Acetylcarnitine C9
Fumarate C2
Glutamate C4
Glutamine C4
Oxoglutarate C4
Glutathione C4
Malate C2
Malate C3
Proline C4

196

197

198 **Fig. 2. AML cells import the secreted acetate in co-culture to use it as a biofuel. a,**
199 Extracellular acetate levels in SKM-1 cells cultured with 0.25 mM and 3 mM acetate medium after 0,
200 24 and 48 hours. Each point represents the mean of n=3 independent experiments and error bars
201 represent standard deviation. An unpaired Student's t-test was applied for each condition (black
202 brackets) and p-values are represented by * for p-value<0.05, ** for p-value<0.01 and *** for p-
203 value<0.001. **b,** Scheme of label distribution arising from [2-^{13}C]acetate in TCA cycle intermediates.
204 Black circles correspond to expected labelled positions. **c,** ^{13}C percentages of label incorporation in
205 polar metabolites from labelled acetate in SKM-1 and MS-5 cells after two hours of incubation with
206 [2-^{13}C]acetate (4 mM) derived from ^{1}H-^{13}C-HSQC NMR spectra. Bars represent the mean of the ^{13}C
207 percentage and error bars represent the standard deviations for n=3 independent experiments. **d,**
208 Experimental design for acetate labelling in co-culture. Briefly, AML cells are co-cultured with
209 stromal cells for 24 hours prior to addition of [2-^{13}C]acetate (extra 4 mM). After 8 hours of the
210 addition of acetate, cells are separated, and metabolites are extracted. **e,** ^{13}C percentages on polar
211 metabolites in SKM-1 and MS-5 cells in co-culture. Cells were co-cultured for 24 hours before the
212 addition of extra 4 mM sodium [2-^{13}C]acetate. Bars represent the mean of the ^{13}C percentage and
213 error bars represent the standard deviations of n=3 independent experiments. For C and E, ^{13}C
214 natural abundance is represented as a black bar at %^{13}C = 1.1.

215

216 **Transcriptomic data highlights a metabolic rewiring of stromal cells in co-culture characterised by**
217 **upregulation of glycolysis and downregulation of pyruvate dehydrogenase**

218 After establishing that stromal cells are responsible for acetate secretion (Fig. 1d) and that AML cells
219 consumed the secreted acetate in co-culture (Fig. 2d), we sought to elucidate the mechanism behind
220 acetate secretion by MS-5 cells in co-culture. Thus, we set out to perform global gene expression
221 profiling by RNA-seq comparing cells cultured alone and in co-culture (Supplementary Fig. 4a). With
222 this approach we identified 587 differentially expressed genes (q-value<0.1) (Supplementary Fig. 4b);
223 with 476 genes being upregulated and 111 genes being downregulated in co-culture.

224 Following clustering of differentially expressed genes, gene set enrichment analysis (GSEA) was
225 performed (Fig. 3a) revealing a positive correlation with the expression of genes that are part of the
226 glycolysis pathway (MSigDB: M5937) as well as the reactive oxygen species pathway (MsigDB:
227 M5938) (Fig. 3b).

228 A closer examination of the genes involved in the glycolysis pathway revealed a major upregulation
229 of several glycolysis-related genes in MS-5 cells in co-culture (Fig. 3c). Most of the genes involved in
230 glucose transport (*Slc2a1* and *Slc2a4*) and glucose breakdown to pyruvate (*Pgm1*, *Hk2*, *Gpi1*, *Pfkl*,
231 *Gapdh*, *Pgk1*, *Pgam1-2*, *Eno1-1b-2* and *Pkm*) were upregulated, including the gene encoding for the
232 6-phosphofructo-2-kinase/fructose-2,6-biphosphatase 3 (*Pfkfb3*), a well-known activator of
233 glycolysis.

234 In contrast, individual examination of genes related to pyruvate metabolism revealed that the genes
235 related to pyruvate conversion to acetyl-CoA were downregulated (Fig. 3c). Pyruvate transport into
236 the mitochondria (*Mpc1-2*) and several pyruvate dehydrogenase (PDH) complex-related genes
237 (*Pdha1*, *Pdhb* and *Pdhx*), involved in the conversion of pyruvate to acetyl-CoA, remained largely
238 unaltered or were slightly downregulated by co-culture. Additionally, the pyruvate dehydrogenase
239 kinases (*Pdk1*, *Pdk2* and *Pdk4*), which inhibit the activity of the PDH complex, were found to be
240 upregulated by co-culture. Interestingly, the acetyl-CoA synthetases (ACSs), which can generate
241 acetyl-CoA from acetate but have also been reported to perform the reverse reaction, encoded by
242 *Acss2* and *Acss3*, were found to be slightly upregulated in co-culture. Pyruvate can also be converted
243 to 2-oxaloacetate via pyruvate carboxylase (*Pcx*), to lactate by lactate dehydrogenase (*Ldha*), and to
244 alanine via alanine transaminase (*Gpt*). Only *Ldha* was found to be moderately upregulated in co-
245 culture. However, we did not observe a substantial increase in lactate production experimentally in
246 co-culture. Altogether, transcriptomic data suggests that MS-5 cells in co-culture present a major
247 upregulation of glycolysis and downregulation of the PDH complex.

248 To explore whether glycolysis is upregulated at a metabolic level in MS-5 cells in co-culture at the
249 metabolic level and whether acetate could derive from glucose, we performed [U-^{13}C]glucose tracing
250 on AML and MS-5 cells cultured alone and in co-culture and analysed the label incorporation in
251 glycolysis-related extracellular metabolites (Fig. 3d). For the three AML cell lines tested, extracellular
252 acetate presented significantly higher label incorporations from [U-^{13}C]glucose in co-culture
253 compared to cell types cultured alone, providing evidence that the secreted acetate in co-culture
254 derives from glucose. Lactate and alanine, which can be synthesised from pyruvate, did not show
255 significant increases in label incorporation from [U-^{13}C]glucose in co-culture compared to each cell
256 type cultured alone for all the AML cell lines, with the exception of alanine in HL-60. Overall, these
257 results are in agreement with the transcriptomic data (Fig. 3c), highlighting that glucose metabolism
258 is upregulated in co-culture but also confirming that acetate derives from glycolysis.

259

3

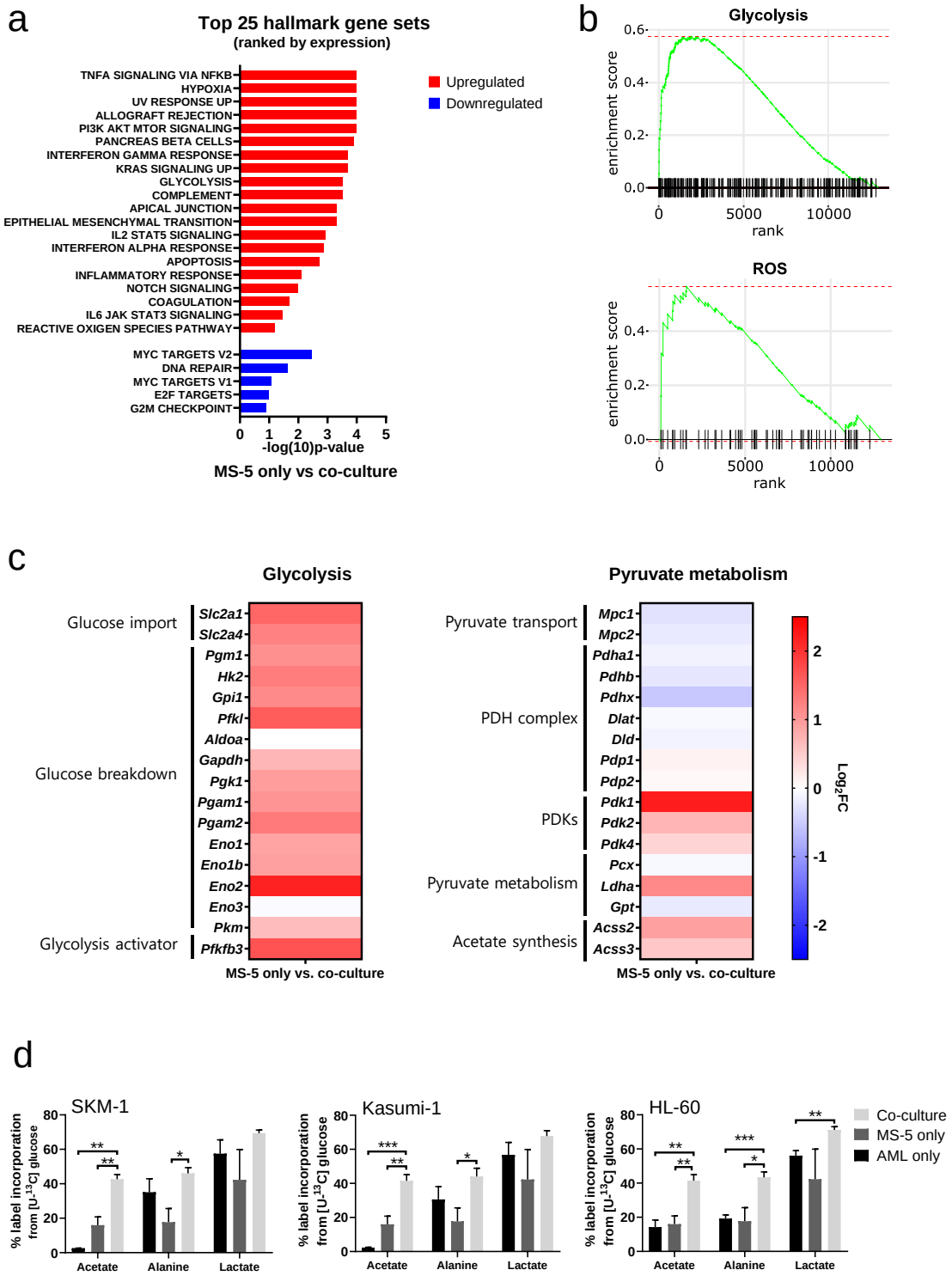
a
Top 25 hallmark gene sets
(ranked by expression)
TNFA SIGNALING VIA NFKB
HYPOXIA
UV RESPONSE UP
ALLOGRAFT REJECTION
PI3K AKT MTOR SIGNALING
PANCREAS BETA CELLS
INTERFERON GAMMA RESPONSE
KRAS SIGNALING UP
GLYCOLYSIS
COMPLEMENT
APICAL JUNCTION
EPITHELIAL MESENCHYMAL TRANSITION
IL2 STAT5 SIGNALING
INTERFERON ALPHA RESPONSE
APOPTOSIS
INFLAMMATORY RESPONSE
NOTCH SIGNALING
COAGULATION
IL6 JAK STAT3 SIGNALING
REACTIVE OXIGEN SPECIES PATHWAY
MYC TARGETS V2
DNA REPAIR
MYC TARGETS V1
E2F TARGETS
G2M CHECKPOINT
Upregulated
Downregulated
-log(10)p-value
MS-5 only vs co-culture
b
Glycolysis
ROS
enrichment score
rank
c
Glycolysis
Glucose import
Glucose breakdown
Glycolysis activator
Slc2a1
Slc2a4
Pgm1
Hk2
Gpi1
Pfkl
Aldoa
Gapdh
Pgk1
Pgam1
Pgam2
Eno1
Eno1b
Eno2
Eno3
Pkm
Pfkfb3
MS-5 only vs. co-culture
Pyruvate metabolism
Pyruvate transport
PDH complex
PDKs
Pyruvate metabolism
Acetate synthesis
Mpc1
Mpc2
Pdha1
Pdhb
Pdhx
Dlat
Dld
Pdp1
Pdp2
Pdk1
Pdk2
Pdk4
Pcx
Ldha
Gpt
Acss2
Acss3
MS-5 only vs. co-culture
Log2FC
d
SKM-1
Kasumi-1
HL-60
% label incorporation from [U-13C] glucose
Acetate
Alanine
Lactate
Co-culture
MS-5 only
AML only

262 **Fig. 3. Transcriptomic data reveals that stromal cell metabolism is shifted towards higher**
263 **glycolysis and ROS upon co-culture with AML cells. a,** Top 25 GSEA hallmark gene sets ranked
264 by expression in MS-5 cells only vs co-culture with SKM-1 cells, analysed using the collection of
265 hallmark gene sets from Molecular Signature Database with a false discovery rate threshold at 5%. P-
266 values for each pathway are presented as –log(10)p-value. **b,** GSEA enrichment score plots of
267 glycolysis and ROS generated using Sleuth 0.30.0 R statistical package. **c,** Fold change values of
268 detected gene transcripts (TPMs) related to glycolysis and pyruvate metabolism. FC values are
269 represented as log_2FC, red values indicate upregulation and blue values indicate downregulation in
270 MS-5 cells in co-culture. **d,** Label incorporation from [U-^{13}C]glucose into extracellular metabolites in
271 AML and MS-5 cells cultured alone or in co-culture after 24 hours. Bars represent the mean of n=3
272 independent experiments and error bars represent standard deviations.

273

274 **AML cells rewire stromal cell metabolism transferring ROS via gap junctions to obtain acetate**

275 Tracer-based data on MS-5 cells in co-culture revealed that acetate secreted in co-culture derives
276 from glucose (Fig. 3d). However, transcriptomic data on MS-5 cells in co-culture suggested that
277 acetate did not derive from pyruvate via acetyl-CoA (Fig. 3c). Moreover, acetate secretion was also
278 observed in MS5 cells grown in thiamine-free media (Supplementary Fig. 5a), confirming that the
279 acetate secretion was not dependent on keto acid dehydrogenases [28] and indicating that a different
280 mechanism must be responsible. An alternative mechanism of acetate synthesis involving a non-
281 enzymatic oxidative decarboxylation of pyruvate into acetate had previously been described [28-30].
282 This mechanism was reported to be mediated by ROS in mammalian cells and was linked to cells
283 prone to overflow metabolism under the influence of high rates of glycolysis and excess pyruvate.
284 Hence, we decided to investigate whether ROS might play a role in acetate secretion in our co-
285 culture system.

286 We first modulated ROS levels in AML cells and MS-5 cells cultured alone and in co-culture and
287 measured acetate production. Hydrogen peroxide was used to increase ROS levels and N-
288 acetylcysteine (NAC) was used as a ROS scavenger. Extracellular acetate levels were measured by ^{1}H-
289 NMR after 24 hours. Increasing ROS levels with peroxide resulted in a significant increase in acetate
290 secretion, particularly in SKM-1 and Kasumi cells in co-culture (Fig. 4a, Supplementary Fig. 5b)). This
291 experiment could not be carried out with HL-60 cells as peroxide treatment severely impaired the
292 viability of HL-60 cells, as previously reported [31]. Additionally, when the ROS scavenger NAC was
293 used, a significant decrease in the levels of acetate in both MS-5 cells cultured alone and in all the
294 co-cultured cell lines was observed (Fig. 4a, Supplementary Fig. 5b). Interestingly, the production of
295 acetate in cells in co-culture treated with NAC recovered the phenotype of MS-5 cells cultured alone,
296 indicating that acetate synthesis in MS-5 cells in co-culture is mediated by ROS (Fig. 4a).

297 Next, we compared intracellular ROS levels in AML and stromal cells in co-culture and cultured alone
298 by labelling cells with the H_2DCFDA fluorescent dye. Fluorescence measurements showed that ROS
299 levels in the three AML cell lines used were significantly decreased in co-culture, whilst in the
300 stromal cells ROS levels were significantly increased in two of the three co-cultures (Fig. 4b). These
301 results suggested that AML cells might transfer ROS to stromal cells. We also performed the same
302 experiment using three primary AML samples to corroborate the previous result. Fluorescence
303 analysis showed decreased ROS levels in AML samples in co-culture and increased ROS levels in MS-5
304 cells in co-culture for the three primary AML samples analysed (Fig. 4c), suggesting ROS transfer
305 from AML cells to stromal cells in co-culture.

306 To further test whether AML cells might transfer ROS through a contact-dependent mechanism, we
307 compared the intracellular ROS levels in AML and stromal cells cultured alone and co-cultured
308 without direct contact using a permeable membrane. Fluorescence measurements in both cell types
309 revealed that ROS levels remained unaltered in contact-free co-cultures (Fig. 4d), indicating that ROS
310 transfer could only occur via a contact-dependent mechanism.

311 As it had been previously reported that haematopoietic stem cells can transfer ROS to stromal cells
312 via gap junctions to prevent senescence [32], we decided to examine gap junction genes in the
313 transcriptome of MS-5 cultured alone and in co-culture. When individually examining the gap
314 junction genes in MS-5 cells cultured alone vs co-culture, we found several gap junction genes
315 upregulated in co-culture such as *Gja5, Gja8, Gjb5* and *Gjc2* (Fig. 4e). These results suggest that AML
316 cells might establish gap junction interactions to transfer ROS to MS-5 cells when in co-culture. To
317 test this hypothesis, we used the calcein-AM dye, which can only be transferred via gap junctions [10].
318 We labelled stromal cells with calcein-AM, cultured them with unlabelled AML cells and analysed the
319 fluorescence of AML cells after three hours. We found that, for the three AML cell lines tested, the
320 percentage of cells that had incorporated the calcein-AM dye from MS-5 cells was larger than 80%
321 (Fig. 4f, Supplementary Fig. 5c), indicating that AML cells can establish gap junctions with stromal
322 cells when co-cultured in direct contact.

323 Next, we decided to confirm that AML cells can transfer ROS via gap junctions by inhibiting the gap
324 junctions using carbenoxolone (CBX), a well-known gap junction inhibitor [10,33,34]. We first confirmed
325 that efficiency of inhibition by analysing the calcein-AM dye transfer in a control and treated co-
326 culture of SKM-1 and MS-5 cells. The CBX treatment reduced the calcein-AM transfer more than 60%
327 in co-culture (Fig. 4g). We then compared intracellular ROS levels in both AML and stromal cells
328 treated with CBX and control. CBX treatment abrogated the decrease in ROS levels in AML cells (Fig.
329 4h) and the increase of ROS levels in stromal cells (Fig. 4i), indicating inhibition of ROS transfer in
330 CBX treated co-cultures. Overall, this result provides strong evidence that ROS transfer occurs via
331 gap junctions established between AML and stromal cells.

332

4

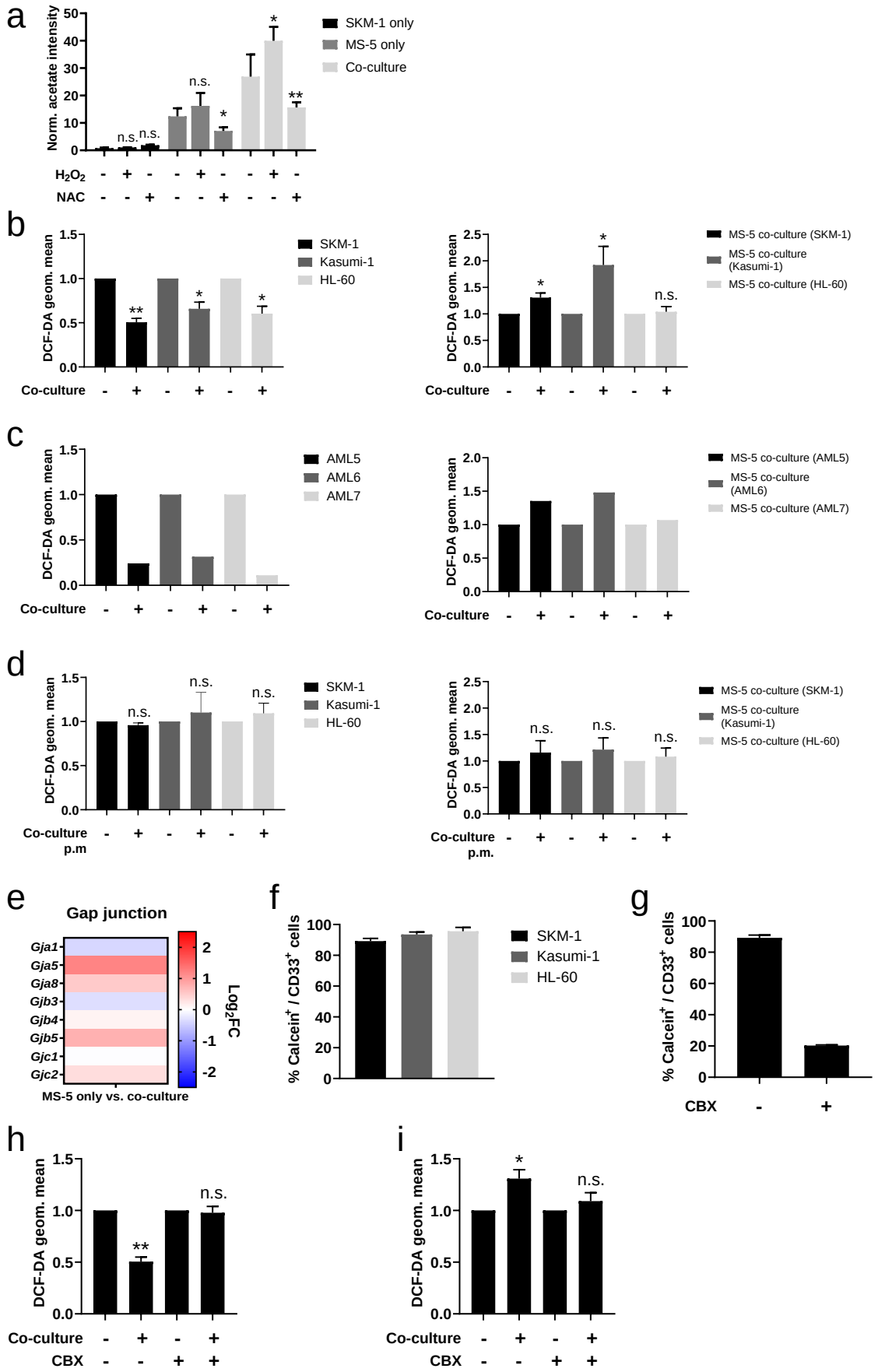
a
Norm. acetate intensity
SKM-1 only
MS-5 only
Co-culture
n.s.
n.s.
n.s.
*
*
**
H2O2 - + - - + - - + -
NAC - - + - - + - - +
b
DCF-DA geom. mean
SKM-1
Kasumi-1
HL-60
Co-culture - + - + - +
MS-5 co-culture (SKM-1)
MS-5 co-culture (Kasumi-1)
MS-5 co-culture (HL-60)
c
AML5
AML6
AML7
MS-5 co-culture (AML5)
MS-5 co-culture (AML6)
MS-5 co-culture (AML7)
d
Co-culture p.m
Co-culture p.m.
e
Gap junction
Gja1
Gja5
Gja8
Gjb3
Gjb4
Gjb5
Gjc1
Gjc2
MS-5 only vs. co-culture
Log2FC
f
% Calcein+ / CD33+ cells
g
CBX - +
h
CBX - - + +
i

333

334 **Fig. 4. Acetate secretion is linked to ROS transfer from AML to stromal cells via gap**
335 **junctions. a,** Extracellular acetate levels in SKM-1 (black) and MS-5 cells cultured alone (dark grey)
336 and in co-culture (light grey) for 24 hours in a control medium, medium with 50 µM H_2O_2 or medium
337 with 5 mM NAC. **b**, **c** and **d** Intracellular ROS levels measured by H_2DCFDA staining in **b** and **d** AML
338 cells or **c** primary patient-derived AML cells and MS-5 cells cultured alone and in co-culture in **b** and **c**
339 direct contact or **e,** fold change values of detected gene transcripts (TPMs) related to gap junctions.
340 FC values are represented as $\log_2$FC, red values indicate upregulation and blue values indicate
341 downregulation in MS-5 cells in co-culture. **f,** Frequencies of Calcein-AM and CD33 positive AML cell
342 lines after being in co-culture with Calcein-AM stained MS-5 cells for 3 hours. **g,** Frequencies of
343 Calcein-AM and CD33 positive SKM-1 cells (treated or untreated with 200 µM carbenoxolone for 24
344 hours) after being in co-culture with Calcein-AM stained MS-5 cells for 3 hours. **h** and **i** Intracellular
345 ROS levels measured by H_2DCFDA staining in AML cells (**h)** and MS-5 cells (**i)** cultured alone and in
346 co-culture in direct contact treated or untreated with 200 µM carbenoxolone for 24 hours. For **a**, **b**,
347 **c**, **d**, **f**, **g**, **h** and **i** bars represent the mean of n=3 independent experiments and error bars represent
348 standard deviations. For **a**, **b**, **d**, **h** and **i** unpaired Student's t-test was applied for **a** each condition
349 (H_2O_2/NAC) was compared to untreated; for **b**, **d**, **h** and **i** co-culture conditions were compared to
350 cells cultured alone. P-values are represented by n.s. for not significant, * for p-value<0.05, ** for p-
351 value<0.01 and *** for p-value<0.001.

352

353 **Discussion**

354 AML cells are known to interact and remodel niche cells through various mechanisms, including the
355 secretion of soluble factors, cytokines or metabolites, resulting in a better support of AML cells at
356 the expense of normal haematopoiesis. Yet, metabolic crosstalk between AML and stromal cells has
357 not been reported before. Here, we have identified a novel metabolic communication between AML
358 and stromal cells mediated by acetate. Our in vivo data using cells from a MLL-AF9 knock-in mouse
359 model showed higher acetate levels in the bone marrow extracellular fluid in leukaemic compared to
360 healthy control mice, indicative of a potential role for acetate in AML development. Our in vitro data
361 suggests that AML cells can modulate stromal cells into secreting acetate in co-culture, by rewiring
362 stromal cell metabolism, and can then utilise the secreted acetate to feed their own TCA cycle to
363 generate energy. Co-cultures with primary cells suggest that this effect could be also occurring in at
364 least a subset of primary AML cells.

365 Mechanistically, our data revealed that acetate secretion involves not only a higher glycolytic rate
366 but also the non-enzymatic ROS-mediated conversion of pyruvate to acetate, as cells grown in
367 thiamine-free media were still capable to produce acetate. Furthermore, our data indicates that
368 AML cells can diminish their ROS levels by establishing gap junctions with stromal cells facilitating
369 ROS transfer to stromal cells.

370 Studying the interactions between cancer cells and their microenvironment in terms of metabolism
371 has become an exciting new field of cancer research. Our data indicates that AML cells can influence
372 the metabolism of stromal cells causing increased acetate secretion, which was not observed in
373 healthy counterparts. We presented several lines of evidence suggesting that stromal cells but not
374 AML cells are responsible for acetate secretion: (i) stromal cells cultured alone secreted acetate,
375 whilst AML cell lines and primary AML cells did not; (ii) after separating stromal cells from co-culture
376 with AML cell lines, stromal cells continued to secrete acetate at a similar rate to that observed in
377 co-culture; and, (iii) glycolysis was upregulated in stromal cells in co-culture, and glucose was found
378 to be the precursor of the secreted acetate in co-culture.

379 Interestingly, acetate has been reported as an alternative fuel for cancer cells [35,36], especially under
380 low oxygen conditions or lipid depletion [37-39], but it has not previously been described to participate
381 in crosstalk between any type of cancer cells and their microenvironment. Nonetheless, other
382 monocarboxylate metabolites, such as lactate and alanine, have been reported to participate in
383 different types of metabolic interplay between stromal and cancer cells [40-42]. Our work reveals that
384 aside from lactate and alanine, other monocarboxylate metabolites, such as acetate, can be utilised
385 by leukaemic cells as a biofuel. Although acetate usage to feed the TCA cycle had already been

386 described in AML [43] and other types of cancer [38,44], this is, to our knowledge, the first report of AML
387 cells utilising acetate secreted by stromal cells in co-culture.

388 We have also proposed a mechanism for the altered stromal cellular metabolism, involving
389 increased glycolysis and the ROS-mediated chemical conversion of pyruvate to acetate.
390 Transcriptomics showed that glycolysis is upregulated in stromal cells in co-culture, and tracer-based
391 metabolism using [U-^{13}C]glucose, demonstrated that more glucose-derived label gets incorporated
392 in pyruvate and acetate in stromal cells in co-culture compared to either AML or stromal cells
393 cultured alone. Enrichment of hypoxia genes and elevated Pdk expression have been reported to be
394 related to higher glycolytic activity [45-47]. Similarly, other cancer cells [48-51] have also been shown to
395 modulate stromal metabolism by increasing glycolysis. Moreover, this mechanism was further
396 supported by modulating ROS levels in co-culture, as increasing or lowering ROS levels had a clear
397 influence on acetate secretion.

398 AML cells are known to exhibit high levels of ROS [52,53]. However, our data has shown that AML cells
399 in co-culture present lower levels of ROS than AML cells cultured alone, which is in agreement with
400 recent studies in primary AML and mesenchymal stromal cell co-cultures [14,24]. The current
401 mechanisms to describe this phenomenon involve mitochondrial transfer and activation of
402 glutathione-related antioxidant pathways [14,24], although previous data on haematopoietic stem cells
403 (HSCs) revealed that HSCs can directly transfer ROS via gap junctions to stromal cells [32]. Interestingly,
404 our data showed that the decrease in ROS levels was counteracted by inhibiting contact using a
405 permeable membrane. We also found several gap junction genes upregulated in stromal cell types in
406 co-culture. Moreover, we prevented ROS transfer from AML to stromal cells by using the gap
407 junction inhibitor CBX [10,33,34]. Thus, our results suggest that ROS transfer via gap junctions, at least
408 partially, mediates the mechanism behind AML cells presenting lower levels of ROS in co-culture.

409 Overall, this work reveals a unique and novel metabolic communication between AML and stromal
410 cells that involves acetate as the main crosstalk metabolite. We showed that AML cells are capable
411 of modulating the metabolism of stromal cells by transferring ROS via gap junctions resulting in an
412 increased secretion of acetate and its subsequent accumulation in the extracellular medium, which
413 correlates with the observation of higher acetate levels in the bone marrow extracellular fluid of
414 AML mice compared to control mice. Furthermore, we found that AML cells consume the secreted
415 acetate and use it as an energy source, by fluxing it into the TCA cycle. We believe our findings
416 provide a better understanding of how AML cells communicate with stromal cells and could serve as
417 a basis for the development of novel therapeutic strategies to target AML cells by modulating gap
418 junction formation as an adjuvant therapy.

419 ## Methods

420 ### Cell lines

421 The human AML cell lines (SKM-1, Kasumi-1 and HL-60), the mouse stromal cell line (MS-5) and the
422 human cervical cancer cell line (HeLa) were cultured in RPMI 1640 media supplemented with 15%
423 (v/v) FBS, 2 mmol/L L-glutamine and 100 U/ml Penicillin/Streptomycin (all from Thermo Fisher
424 Scientific). Co-cultures were plated in a 4:1 AML-stromal ratio, and 750.000 cells/ml density of AML
425 cells over confluent stromal cells. Prior to cell extraction for NMR, RNA collection or protein
426 extraction, a suspension of 10 million AML cells was collected, the stromal layer was washed with
427 PBS and was subject to mild trypsinisation with 1:5 dilution of 0.25% Trypsin 1 mM EDTA
428 (Thermofisher) to remove attached residual leukaemic cells before completely detaching stromal
429 cells with 0.25% Trypsin-EDTA.

430 ### Primary patient samples

431 AML and PBMC primary specimens' procedures were obtained in accordance with the Declaration of
432 Helsinki at the University Medical Center Groningen, approved by the UMCG Medical Ethical
433 Committee or at the University Hospital Birmingham NHS Foundation Trust, approved by the West
434 Midlands – Solihull Research Ethics Committee (10/H1206//58).

435 Additional information about the primary AML samples used in this study can be found in Annex 1.
436 Peripheral blood (PB) and bone marrow samples from AML patients and healthy donors were
437 obtained in heparin-coated vacutainers. Mononuclear cells were isolated using Ficoll-Paque (GE
438 Healthcare) and stored at -80°C.

439 For AML1-2 and PBMC1-2, samples were thawed and resuspended in newborn calf serum (NCS)
440 supplemented with DNase I (20 Units/mL), 4 mM $MgSO_4$ and heparin (5 Units/mL) and incubated on
441 37°C for 15 minutes (min). For AML1 and PBMC1, cells were sorted after thawing by fluorescence-
442 activated cell sorting (FACS) for the CD34+CD38- population using 10 µL of anti-CD34 APC (560940,
443 BD Biosciences), 10 µL of anti-CD38 FITC (555459, BD Biosciences) and 10 µL of DAPI (D1306, Thermo
444 Fisher Scientific) per 10 million cells. Cells were sorted using a Sony SH800S (Sony) sorter. For AML2
445 and PBMC2, cells were thawed and the CD34+ population was sorted by magnetic-activated cell
446 sorting (MACS) using 10 µL of anti-CD34 microbeads (130-046-702, Miltenyi) per million of expected
447 CD34 cells following manufacturer's protocol.

448 AML1-2, PBMC1-2 and MS-5 cells were cultured alone and in co-culture in a 4:1 AML/PBMC-stromal
449 ratio and 500,000 cells/mL density in α-MEM (Gibco) with 12.5% (v/v) FCS (Sigma-Aldrich), 1% (v/v)

450 Pen/Strep (Thermo Fisher Scientific), 12.5% (v/v) Horse serum (Invitrogen), 0.4% (v/v) β-
451 mercaptoethanol (Merck Sharp & Dohme BV) and 0.1% hydrocortisone (H0888, Sigma-Aldrich). For
452 AML1 and AML2 the medium was supplemented with 0.02 µg/mL of IL-3 (Sandoz), 0.02 µg/mL
453 NPlate (Amgen) and 0.02 µg/mL of G-CSF (Amgen). For PBMC1 and PBMC2 the medium was
454 supplemented with 100 ng/ml of human SCF (255-SC, Novus Biologicals), 100 ng/ml of NPlate, 100
455 ng/ml of FLT3 ligand (Amgen) and 20 ng/ml of IL-3. Samples of medium were collected at 0 and 48
456 hours.

457 AML3 - 7 and PBMC3 were thawed and kept in culture for 16-24 hours in Stem Span H3000 media
458 (STEMCELL Technologies) supplemented with 50 µg/ml ascorbic acid (Sigma-Aldrich), 50 ng/ml
459 human SCF (255-SC-010, R&D Systems), 10 ng/ml human IL-3 (203-IL-010, R&D Systems), 2 units/ml
460 human-erythropoietin (100-64, PeproTech), 40 ng/ml insulin-like growth factor 1 (IGF-1) (100-12,
461 PeproTech), 1 µM dexamethasone (D2915, Sigma-Aldrich) and 100 µg/ml primocin (ant-pm-2,
462 InvivogenCD34+ cKit+ cells were purified using magnetic microbeads (130-046-702 (CD34) and 130-
463 091-332 (CD117), Miltenyi Biotec). Cells were cultured in the supplemented Stem Span media for 24
464 hours prior to co-culture setting. Co-cultures were plated with a 4:1 leukaemic to stromal cells ratio
465 and a 300,000 cells/ml density in supplemented Stem Span medium. Samples of leukaemic/healthy
466 cells and MS-5 cells alone were also cultured in supplemented Stem Span media as controls. Samples
467 of medium were collected at 0 and 48 hours.

468 **In vivo experiments**

469 12 weeks old C57BL6/J female mice (The Jackson Laboratory) were lethally irradiated with 9Gy (2
470 doses of 4.5Gy separated by 3h) using an X-RAY source (Rad Source's RS 2000). Mice were
471 transplanted by intravenous injection 4h after with $2x10^6$ bone marrow (BM) nucleated cells isolated
472 as previously described [54] from leukemic male mice heterozygous for MLL-AF9 knock-in fusion
473 transgene or wild-type (WT) control male littermates [55] . Male transgenic and WT control MLL-AF9
474 were purchased from The Jackson Laboratory (Stock No: 009079) and were 6 months old when
475 euthanized to allow development of signs of leukemic transformation driven by the MLL-AF9 fusion
476 oncogene in transgenic animals. MLL-AF9 expression in BM cells derived from transgenic donors
477 results in development of AML with high blast counts in recipients. Recipients were euthanized 6
478 months after the transplant, bone marrow from femur and tibia was flushed with a syringe in 150 µL
479 of cold PBS and centrifuged at 15000g for 10 minutes at 4^oC. The supernatant made of bone marrow
480 extracellular fluid (BMEF) was kept for analysis of acetate level. Experiments were conducted with
481 the ethical approval of the Norwegian Food and Safety Authority. Animals were housed under

482 specific opportunistic and pathogen free environment at the Animal Facility of the University of Oslo,
483 Norway.

484

485 **Proliferation analysis using CFSE**

486 The CellTrace™ carboxyfluorescein succinimidyl ester (CFSE) Cell Proliferation Kit (C34570,
487 Invitrogen) was used to assess proliferation of AML cells following the manufacturer's protocol. AML
488 cells were stained and their fluorescence was assessed before dividing the bulk of cells into culturing
489 them alone or with MS-5 cells for 48 hours. Small aliquots of cells after 24 and 48 hours were
490 analysed by flow cytometry. Flow cytometry analysis was carried out in a CyAn ADP flow cytometer
491 (Beckman Coulter). Data analysis was performed using the FlowJo software package (BD).

492 **Carbenoxolone treatment**

493 Carbenoxolone (CBX) disodium salt (Sigma-Aldrich, C4790) was prepared fresh at 200 µM in cell
494 culture medium. Cells were resuspended in the CBX medium and cultured alone or in co-culture for
495 24 hours prior to ROS or Calcein-AM dye transfer experiments.

496 **Cellular ROS measurements using DCFH-DA**

497 Cellular ROS was measured by incubating cells with 100 µM 2',7'-Dichlorofluorescin diacetate (DCFH-
498 DA) (D6883, Sigma-Aldrich) in Hank's Balanced Salt Solution (HBSS) (Thermo Fisher Scientific) at 37°C
499 for 30 min protected from light. Cells were then harvested and stained with 5 µg/µL anti-human
500 CD33 eFluor 450 (eBioscience, P67.6) for 30 min at 4°C before flow cytometry analysis as previously
501 described.

502 **Thiamine-free medium comparison**

503 Thiamine-free medium (R9011-01, United States Biological) was prepared as per manufacturer
504 instructions and supplemented with 10% dialised FBS.

505 MS-5 cells were cultured in thiamine-free medium or control RPMI medium for 4 days prior to the
506 experiment. Cells were then seeded with fresh thiamine-free or control RPMI medium and incubated
507 for 24 hours. Samples of medium were collected at 0 and 24 hours and kept at -80ºC.

508 **ROS-related treatments with H_2O_2 and NAC**

509 SKM-1, Kasumi, HL-60 and MS-5 cells cultured alone and in co-culture were incubated for 24 hours in
510 50 µM H_2O_2 (Merck) complete cell culture medium, 5 mM N-acetylcysteine (NAC) (106425, Merck)

511 complete cell culture medium or control medium. Samples of medium were collected at 0 and 24
512 hours and kept at -80°C.

513

514 **Calcein-AM dye transfer assay**

515 Functional gap junction presence was evaluated using the fluorescent dye Calcein-AM green
516 (Invitrogen, C1430) adapting a previously established protocol [10]. MS-5 cells were stained with 500
517 nM Calcein-AM dye in complete cell culture medium for 1 hour at 37°C. Stained cells were washed
518 with serum-free medium for 30 min at 37°C before being co-cultured with AML cells for 3h. AML
519 cells were then harvested and stained with 5 µg/µL anti-human CD33 eFluor 450 (eBioscience,
520 P67.6) for 30 min at 4°C before flow cytometry analysis as previously described. Calcein-AM dye
521 transfer was quantified as the frequency of $CD33^+$ and Calcein-AM^+ cells.

522 **Tracer-based NMR experiments**

523 [U-^{13}C]Glucose (CC860P1, CortecNet) was added to RPMI 1640 medium without glucose (11879020,
524 Merck) to a final concentration of 2 g/L (as in the complete cell culture medium) and was
525 supplemented as usual with 15% (v/v) FBS, 2 mmol/L L-glutamine and 100 U/mL Pen/Strep. The
526 medium was prepared fresh and was filtered with a 0.2 µm syringe filter (Sartorius) before each
527 experiment.

528 4 mM sodium [2-^{13}C]acetate (279315-1G, Sigma-Aldrich) was added to complete cell culture medium
529 and the medium was filtered with a 0.2 µm syringe filter before each experiment. Cells were
530 incubated for the time indicated in each experiment before separation of cells and/or metabolite
531 extraction. **a**, **b**, **c**, **d**, **f**, **g**, **h** and **i** Unlabelled samples were prepared as a control for 2D-NMR
532 experiments and to measure acetate consumption by adding unlabelled sodium acetate trihydrate
533 (1.37012, Merck) to complete cell culture medium before metabolite extraction or collection of
534 medium samples.

535 **Metabolite extraction**

536 Suspension cells and detached adherent cells were washed with PBS before being rapidly
537 resuspended in 400 µl of HPLC grade methanol pre-chilled on dry ice. Samples were transferred to
538 glass vials and were subject to 10:8:10 methanol-water-chloroform extraction as described in
539 (Saborano 2019). Polar phase samples were evaporated in a SpeedVac concentrator and were
540 subsequently kept at -80°C.

541 **Sample preparation for NMR**

542 Medium samples or bone marrow extracellular fluid samples were mixed with a D_2O phosphate
543 buffer containing TMSP ((3-trimethylsilyl)propionic-(2,2,3,3-d_4)-acid sodium salt) and NaN_3 to a final
544 concentration of 0.1 M phosphate and 0.5 mM TMSP (3-trimethylsilyl)propionic-(2,2,3,3-d_4)-acid
545 sodium salt) and 1.5 mM NaN_3 (all from Sigma) and transferred to 3 mm NMR tubes (Cortecnet).

546 Dried polar extracts for tracer-based NMR experiments were reconstituted in 50 µL of 0.1 M
547 phosphate buffer in 100% D_2O with 3 mM NaN_3 and 0.5 mM TMSP. Samples were sonicated for 10
548 min and transferred to 1.7 mm NMR tubes using a micro pipet system. Samples were prepared
549 freshly before the acquisition.

550 **NMR acquisition and analysis**

551 All NMR data were acquired on Bruker 600MHz spectrometers equipped with Avance-III consoles
552 using cooled Bruker SampleJet autosamplers. For media samples, a 5mm triple resonance cryoprobe
553 (TCI) z-axis pulsed field gradient (PFG) cryogenic probe was used, and for cell extracts, a TCI 1.7mm
554 z-PFG cryogenic probe was used. Probes were equipped with a cooled SampleJet autosampler
555 (Bruker) and automated tuning and matching.

556 For medium samples, spectra were acquired at 300K using 1D ^{1}H-NOESY (Nuclear Overhauser effect
557 spectroscopy) pulse sequence with pre-saturation water suppression (noesygppr1d, standard pulse
558 sequence from Bruker). The spectral width was 12 ppm, the number of data points was TD 32,768,
559 the interscan delay was 4 sec and the NOE mixing time was 10 msec. The ^{1}H carrier was set on the
560 water frequency and the ^{1}H 90º pulse was calibrated at a power of 0.256 W and had a typical length
561 of ca 7-8 µs. 64 scans and 8 dummy scans were acquired and the total experimental time was 7.5
562 min. Spectra were processed using the MetaboLab [56] software within the MATLAB environment
563 (MathWorks). A 0.3Hz exponential apodization function was applied to FIDs followed by zero-filling
564 to 131,072 data points prior to Fourier transformation. The chemical shift was calibrated by
565 referencing the TMSP signal to 0 ppm and spectra were manually phase corrected. The baseline was
566 corrected by applying a spline baseline correction, the water and edge regions of the spectra were
567 excluded before scaling the spectra using a probabilistic quotient normalization (PQN). Chenomx 7.0
568 software (Chenomx Inc.) and the human metabolome database (HMDB) were used to assign the
569 metabolites present in the acquired spectra. Metabolite signal intensities were obtained directly
570 from the spectra and were normalised to a control medium sample obtained at time 0 hours. For
571 bone marrow extracellular fluid samples, metabolite signal areas were obtained directly from the
572 spectra.

573 For ^{13}C-filtered ^{1}H-NMR experiments, [U-^{13}C]glucose labelled medium samples were analysed with
574 ^{13}C-filtered ^{1}H-NMR spectroscopy as described in [57]. Spectra were acquired at 300 K using a double
575 gradient BIRD filter pulse sequence developed in-house [57]. A pulse program combining the ^{1}H[^{12}C]
576 and the all-^{1}H experiments in scan-interleaved mode was used. The difference between the two FIDs
577 gave the ^{1}H[^{13}C] signal. The spectral width was 12 ppm, the number of data points was 16,384 in
578 each dimension and the relaxation delay was 5.3 sec. 256 scans with 64 dummy scans were acquired
579 and the experimental time was 15 min. ^{13}C-filtered ^{1}H-NMR spectra were processed in Topspin 4.0.5
580 (Bruker). Spectra were zero filled to 32,768 data points before Fourier transformation. Phase
581 correction was applied to the ^{1}H[-^{12}C] and the all-^{1}H spectra and the difference ^{1}H[^{13}C] spectrum was
582 obtained by aligning on chemical shift. Metabolites were selected in the ^{1}H[^{13}C] spectrum and
583 integrated in all the spectra (^{1}H[^{12}C], ^{1}H[^{13}C] and all-^{1}H). Label incorporations (^{13}C percentages) were
584 calculated by dividing the signal areas obtained in the ^{1}H[^{13}C] spectrum by the ones obtained in the
585 all-^{1}H spectrum.

586 For ^{1}H-^{13}C-HSQC experiments, spectra were acquired using a modified version of Bruker's
587 hsqcgphprsp pulse program, with additional gradient pulses during the INEPT echo periods and using
588 soft 180º pulses for ^{13}C. For the ^{1}H dimension, the spectral width was 13.018 ppm with 2048
589 complex points. For the ^{13}C dimension, the spectral width was 160 ppm with 2048 complex points. 2
590 scans were acquired per spectrum and with an interscan delay of 1.5 sec. Non-uniform sampling
591 (NUS) with a 25% sampling schedule (generated using the Wagner's schedule generator (Gerhard
592 Wagner Lab, Harvard Medical School) with a tolerance of 0.01 and default values for the other
593 parameters) was used with 4096 increments yielding 8192 complex points after processing. The total
594 experimental time was 4 hours. Spectra were processed and phased with NMRPipe (National
595 Institute of Standards and Technology of the U.S.) (Appendix 8.1). MetaboLab was used to reference
596 the chemical shift using the signal for the methyl group of L-lactic acid, at 1.31/22.9 ppm in the ^{1}H
597 and ^{13}C dimensions, respectively. Identification of metabolites in 2D spectra was carried out using
598 the MetaboLab software which includes a chemical shift library for ca. 200 metabolites. Intensities
599 were obtained from signals in the spectra and were corrected for differences in cell numbers
600 contributing to the sample as follows: A ^{1}H-NMR spectrum was acquired for each sample and the
601 total metabolite area of this spectrum after removal of the water and TMSP reference signal was
602 calculated in MetaboLab. The intensities in the 2D spectra were then divided by the total metabolite
603 area of the corresponding ^{1}H-NMR spectrum. To obtain the % of ^{13}C in a metabolite, the normalized
604 intensity of a certain carbon in the labelled sample was divided by the normalized intensity of the
605 same carbon in the unlabelled sample and was multiplied by the natural abundance of ^{13}C (1.1%).

606 **RNA extraction and sequencing**

607 MS-5 cells were cultured alone or in co-culture with SKM-1 cells for 24 hours. Cells were separated
608 and washed with PBS prior to RNA extraction with TRIzol (Gibco) according to the manufacturer's
609 protocol. RNA was purified with RNeasy Plus Micro kit. Samples were sent to Theragenetex to be
610 sequenced with Novaseq 150bp PE with 40M reads.

611

612 **Real-time PCR**

613 Samples of RNA from SKM-1 and MS-5 co-cultures were collected and extracted using Trizol
614 (Invitrogen) following manufacturer's protocol. cDNA was synthesized using the M-MLV reverse
615 transcriptase (Promega) according to manufacturer's instructions. For gene expression analysis, qRT-
616 PCR of *Hk2* (NM_013820), *Pdhx* (NM_175094), *Pdk1* (NM_172665) and *Pdk2* (NM_133667) (all
617 KiCqStart™ primers KSPQ12012, Sigma Aldrich) were carried out using the SYBRGreen Master mix
618 (Thermo Fisher Scientific) and qRT-PCR of *B2m* (NM_009735.3, TaqMan® assays, Thermo Fisher
619 Scientific) was performed using TaqMan PCR Master Mix (Thermo Fisher Scientific). Reactions were
620 performed in a Stratagene Mx3000P and were run in triplicate. Relative gene expression was
621 calculated following the $2^{-\Delta\Delta Ct}$ method relative to the expression of *B2m*.

622 **RNA sequencing**

623 RNA samples of MS-5 cells cultured alone and in co-culture with SKM-1 cells extracted using Trizol
624 were purified using the Rneasy Plus Micro kit (Qiagen) according to manufacturer's protocol.
625 Transcriptome analysis was performed by Theragen Etex Co., LTD. (www.theragenetex.net). cDNA
626 libraries were prepared with the TruSeq Stranded mRNA Sample Prep Kit (Illumina) and RNA
627 sequencing was performed in a HiSeq2500 platform (Illumina). Quality control metrics were
628 obtained with FastQC 0.11.7 software (Babraham Bioinformatics). To quantify transcript abundances
629 using the Kallisto 0.43.0 software (Patcher Lab), read counts were aligned to the GRCm38 mouse
630 reference genome cDNA index (Ensembl rel.67). Gene-level differential expression analysis was
631 carried out with the R statistical package Sleuth 0.30.0 comparing the expression of cells cultured
632 alone vs co-culture. Differentially expressed genes were calculated using the Wald statistical test,
633 correcting for multiple testing with the Benjamin-Hochberg method. The false discovery rate (FDR)
634 threshold was set at 1% (q-values < 0.01). Ensembl gene transcripts were annotated to Entrez IDs
635 and official gene symbols with the R statistical package BioMart 2.40.3. To normalise for sequencing
636 depth and gene length, transcripts per million (TPM) expression values were calculated. Gene Set
637 Enrichment Analysis (GSEA) was performed with the R statistical package fgsea 1.10.0. The collection

638 of hallmark gene sets from the Molecular Signature Database was used for the GSEA, setting the FDR
639 threshold at 5%. Data was deposited in GEO (GSE163478).

640

641 **References**

642 1. Kreitz, J.*, et al.* Metabolic Plasticity of Acute Myeloid Leukemia. *Cells* **8**(2019).
643 2. Schelker, R.C.*, et al.* TGF-β1 and CXCL12 modulate proliferation and chemotherapy
644 sensitivity of acute myeloid leukemia cells co-cultured with multipotent mesenchymal
645 stromal cells. *Hematology* **23**, 337-345 (2018).
646 3. Passaro, D.*, et al.* Increased Vascular Permeability in the Bone Marrow Microenvironment
647 Contributes to Disease Progression and Drug Response in Acute Myeloid Leukemia. *Cancer*
648 *Cell* **32**, 324-341 e326 (2017).
649 4. Zeng, Z.*, et al.* Inhibition of CXCR4 with the novel RCP168 peptide overcomes stroma-
650 mediated chemoresistance in chronic and acute leukemias. *Mol Cancer Ther* **5**, 3113-3121
651 (2006).
652 5. Carey, A.*, et al.* Identification of Interleukin-1 by Functional Screening as a Key Mediator of
653 Cellular Expansion and Disease Progression in Acute Myeloid Leukemia. *Cell reports* **18**,
654 3204-3218 (2017).
655 6. Zhang, T.Y.*, et al.* IL-6 blockade reverses bone marrow failure induced by human acute
656 myeloid leukemia. **12**, eaax5104 (2020).
657 7. Wang, B.*, et al.* Exosomes derived from acute myeloid leukemia cells promote
658 chemoresistance by enhancing glycolysis-mediated vascular remodeling. *J Cell Physiol* **234**,
659 10602-10614 (2019).
660 8. Kumar, B.*, et al.* Acute myeloid leukemia transforms the bone marrow niche into a leukemia-
661 permissive microenvironment through exosome secretion. *Leukemia* **32**, 575-587 (2018).
662 9. Hornick, N.I.*, et al.* AML suppresses hematopoiesis by releasing exosomes that contain
663 microRNAs targeting c-MYB. *Science signaling* **9**, ra88 (2016).
664 10. Kouzi, F.*, et al.* Disruption of gap junctions attenuates acute myeloid leukemia
665 chemoresistance induced by bone marrow mesenchymal stromal cells. *Oncogene* **39**, 1198-
666 1212 (2020).
667 11. Omsland, M., Bruserud, Ø., Gjertsen, B.T. & Andresen, V. Tunneling nanotube (TNT)
668 formation is downregulated by cytarabine and NF-κB inhibition in acute myeloid leukemia
669 (AML). *Oncotarget* **8**, 7946-7963 (2017).
670 12. Ye, H.*, et al.* Leukemic Stem Cells Evade Chemotherapy by Metabolic Adaptation to an
671 Adipose Tissue Niche. *Cell Stem Cell* **19**, 23-37 (2016).
672 13. Moschoi, R.*, et al.* Protective mitochondrial transfer from bone marrow stromal cells to
673 acute myeloid leukemic cells during chemotherapy. *Blood* **128**, 253-264 (2016).
674 14. Forte, D.*, et al.* Bone Marrow Mesenchymal Stem Cells Support Acute Myeloid Leukemia
675 Bioenergetics and Enhance Antioxidant Defense and Escape from Chemotherapy. *Cell Metab*
676 **32**, 829-843 e829 (2020).
677 15. Shafat, M.S.*, et al.* Leukemic blasts program bone marrow adipocytes to generate a
678 protumoral microenvironment. *Blood* **129**, 1320-1332 (2017).
679 16. Tabe, Y.*, et al.* Bone Marrow Adipocytes Facilitate Fatty Acid Oxidation Activating AMPK and
680 a Transcriptional Network Supporting Survival of Acute Monocytic Leukemia Cells. *Cancer*
681 *Res* **77**, 1453-1464 (2017).
682 17. Baccelli, I.*, et al.* Mubritinib Targets the Electron Transport Chain Complex I and Reveals the
683 Landscape of OXPHOS Dependency in Acute Myeloid Leukemia. *Cancer Cell* **36**, 84-99.e88
684 (2019).
685 18. Pollyea, D.A.*, et al.* Venetoclax with azacitidine disrupts energy metabolism and targets
686 leukemia stem cells in patients with acute myeloid leukemia. *Nat Med* **24**, 1859-1866 (2018).
687 19. Molina, J.R.*, et al.* An inhibitor of oxidative phosphorylation exploits cancer vulnerability.
688 *Nature Medicine* **24**, 1036-1046 (2018).
689 20. Lagadinou, E.D.*, et al.* BCL-2 inhibition targets oxidative phosphorylation and selectively
690 eradicates quiescent human leukemia stem cells. *Cell Stem Cell* **12**, 329-341 (2013).

691 21. Farge, T.*, et al.* Chemotherapy-Resistant Human Acute Myeloid Leukemia Cells Are Not
692 Enriched for Leukemic Stem Cells but Require Oxidative Metabolism. *Cancer Discov* **7**, 716-
693 735 (2017).
694 22. Li, L.*, et al.* Altered Hematopoietic Cell Gene Expression Precedes Development of Therapy-
695 Related Myelodysplasia/Acute Myeloid Leukemia and Identifies Patients at Risk. *Cancer Cell*
696 **20**, 591-605 (2011).
697 23. Hole, P.S.*, et al.* Overproduction of NOX-derived ROS in AML promotes proliferation and is
698 associated with defective oxidative stress signaling. *Blood* **122**, 3322-3330 (2013).
699 24. Vignon, C.*, et al.* Involvement of GPx-3 in the Reciprocal Control of Redox Metabolism in the
700 Leukemic Niche. *Int J Mol Sci* **21**(2020).
701 25. Itoh, K.*, et al.* Reproducible establishment of hemopoietic supportive stromal cell lines from
702 murine bone marrow. *Exp Hematol* **17**, 145-153 (1989).
703 26. Childress, C.C., Sacktor, B. & Traynor, D.R. Function of carnitine in the fatty acid oxidase-
704 deficient insect flight muscle. *J Biol Chem* **242**, 754-760 (1967).
705 27. Stephens, F.B., Constantin-Teodosiu, D. & Greenhaff, P.L. New insights concerning the role of
706 carnitine in the regulation of fuel metabolism in skeletal muscle. *J Physiol* **581**, 431-444
707 (2007).
708 28. Liu, X.*, et al.* Acetate Production from Glucose and Coupling to Mitochondrial Metabolism in
709 Mammals. *Cell* **175**, 502-513 e513 (2018).
710 29. Vysochan, A., Sengupta, A., Weljie, A.M., Alwine, J.C. & Yu, Y. ACSS2-mediated acetyl-CoA
711 synthesis from acetate is necessary for human cytomegalovirus infection. *Proc Natl Acad Sci*
712 *U S A* **114**, E1528-E1535 (2017).
713 30. Tiziani, S.*, et al.* Metabolomic profiling of drug responses in acute myeloid leukaemia cell
714 lines. *PLoS One* **4**, e4251 (2009).
715 31. Nogueira-Pedro, A.*, et al.* Hydrogen peroxide (H2O2) induces leukemic but not normal
716 hematopoietic cell death in a dose-dependent manner. *Cancer Cell International* **13**, 123
717 (2013).
718 32. Taniguchi Ishikawa, E.*, et al.* Connexin-43 prevents hematopoietic stem cell senescence
719 through transfer of reactive oxygen species to bone marrow stromal cells. *Proc Natl Acad Sci*
720 *U S A* **109**, 9071-9076 (2012).
721 33. Davidson, J.S., Baumgarten, I.M. & Harley, E.H. Reversible inhibition of intercellular
722 junctional communication by glycyrrhetinic acid. *Biochem Biophys Res Commun* **134**, 29-36
723 (1986).
724 34. Davidson, J.S. & Baumgarten, I.M. Glycyrrhetinic acid derivatives: a novel class of inhibitors
725 of gap-junctional intercellular communication. Structure-activity relationships. *J Pharmacol*
726 *Exp Ther* **246**, 1104-1107 (1988).
727 35. Lyssiotis, C.A. & Cantley, L.C. Acetate fuels the cancer engine. *Cell* **159**, 1492-1494 (2014).
728 36. Comerford, S.A.*, et al.* Acetate dependence of tumors. *Cell* **159**, 1591-1602 (2014).
729 37. Gao, X.*, et al.* Acetate functions as an epigenetic metabolite to promote lipid synthesis under
730 hypoxia. *Nat Commun* **7**, 11960 (2016).
731 38. Schug, Z.T.*, et al.* Acetyl-CoA synthetase 2 promotes acetate utilization and maintains cancer
732 cell growth under metabolic stress. *Cancer Cell* **27**, 57-71 (2015).
733 39. Yoshii, Y.*, et al.* Cytosolic acetyl-CoA synthetase affected tumor cell survival under hypoxia:
734 the possible function in tumor acetyl-CoA/acetate metabolism. *Cancer Sci* **100**, 821-827
735 (2009).
736 40. Sousa, C.M.*, et al.* Pancreatic stellate cells support tumour metabolism through autophagic
737 alanine secretion. *Nature* **536**, 479-483 (2016).
738 41. Sonveaux, P.*, et al.* Targeting lactate-fueled respiration selectively kills hypoxic tumor cells in
739 mice. *J Clin Invest* **118**, 3930-3942 (2008).

740 42. Whitaker-Menezes, D.*, et al.* Evidence for a stromal-epithelial "lactate shuttle" in human
741 tumors: MCT4 is a marker of oxidative stress in cancer-associated fibroblasts. *Cell Cycle* **10**,
742 1772-1783 (2011).
743 43. Saborano, R.*, et al.* A framework for tracer-based metabolism in mammalian cells by NMR.
744 *Sci Rep* **9**, 2520 (2019).
745 44. Mashimo, T.*, et al.* Acetate is a bioenergetic substrate for human glioblastoma and brain
746 metastases. *Cell* **159**, 1603-1614 (2014).
747 45. Testa, U., Labbaye, C., Castelli, G. & Pelosi, E. Oxidative stress and hypoxia in normal and
748 leukemic stem cells. *Experimental Hematology* **44**, 540-560 (2016).
749 46. Kocabas, F.*, et al.* Hypoxic metabolism in human hematopoietic stem cells. *Cell & bioscience*
750 **5**, 39 (2015).
751 47. Takubo, K.*, et al.* Regulation of glycolysis by Pdk functions as a metabolic checkpoint for cell
752 cycle quiescence in hematopoietic stem cells. *Cell Stem Cell* **12**, 49-61 (2013).
753 48. Shan, T.*, et al.* Cancer-associated fibroblasts enhance pancreatic cancer cell invasion by
754 remodeling the metabolic conversion mechanism. *Oncol Rep* **37**, 1971-1979 (2017).
755 49. Migneco, G.*, et al.* Glycolytic cancer associated fibroblasts promote breast cancer tumor
756 growth, without a measurable increase in angiogenesis: evidence for stromal-epithelial
757 metabolic coupling. *Cell Cycle* **9**, 2412-2422 (2010).
758 50. Pavlides, S.*, et al.* The reverse Warburg effect: aerobic glycolysis in cancer associated
759 fibroblasts and the tumor stroma. *Cell Cycle* **8**, 3984-4001 (2009).
760 51. Cruz-Bermudez, A.*, et al.* Cancer-associated fibroblasts modify lung cancer metabolism
761 involving ROS and TGF-beta signaling. *Free Radic Biol Med* **130**, 163-173 (2019).
762 52. Hole, P.S.*, et al.* Overproduction of NOX-derived ROS in AML promotes proliferation and is
763 associated with defective oxidative stress signaling. *Blood* **122**, 3322-3330 (2013).
764 53. Robinson, A.J.*, et al.* Reactive Oxygen Species Drive Proliferation in Acute Myeloid Leukemia
765 via the Glycolytic Regulator PFKFB3. *Cancer Res* **80**, 937-949 (2020).
766 54. Arranz, L.*, et al.* Neuropathy of haematopoietic stem cell niche is essential for
767 myeloproliferative neoplasms. *Nature* **512**, 78-81 (2014).
768 55. Corral, J.*, et al.* An Mll-AF9 fusion gene made by homologous recombination causes acute
769 leukemia in chimeric mice: a method to create fusion oncogenes. *Cell* **85**, 853-861 (1996).
770 56. Ludwig, C. & Gunther, U.L. MetaboLab--advanced NMR data processing and analysis for
771 metabolomics. *BMC Bioinformatics* **12**, 366 (2011).
772 57. Reed, M.A.C., Roberts, J., Gierth, P., Kupce, E. & Gunther, U.L. Quantitative Isotopomer Rates
773 in Real-Time Metabolism of Cells Determined by NMR Methods. *Chembiochem* **20**, 2207-
774 2211 (2019).

775

776

Acknowledgements

N. Vilaplana-Lopera, G. Papatzikas, A. Cunningham, and A. Erdem were supported by the EU grant HaemMetabolome H2020-MSCA-ITN-2015-675790. U. Günther, P. Garcia, J. J. Schuringa, J.-B. Cazier, and F. Schnütgen acknowledge support from the European Commission (HaemMetabolome [EC-675790]). This work was further supported by the Deutsche Forschungsgemeinschaft (DFG, German Research foundation) SFB815, TP A10 (F.S.). We also acknowledge the Wellcome Trust for supporting access to NMR instruments at the Henry Wellcome Building for Biomolecular NMR in Birmingham (grant number 208400/Z/17/Z). The mouse work was supported by a joint meeting grant of the Northern Norway Regional Health Authority and UiT (2014/5668) to L. Arranz. We thank A. Villatoro and L.M. Gonzalez for technical assistance.

Author Contributions

N.V-L. conceived and performed the experiments, acquired, analysed and interpreted the data, and wrote the manuscript. V.C., R.A., E.G., A.C., A.E., F.S., M.R., L.A. performed the experiments and edited the manuscript. G.P. analysed the RNA-seq data. J.B helped with the experimental design. S.P. and M.R. provided with patient samples. V.C. and L.A. provided mouse bone marrow extracellular fluid samples. J.J.S. provided patient samples, helped with the experimental design, interpretation and critical discussion of the data and edited the manuscript. U.G and P.G. conceived and performed the experiments, acquired and interpreted the data, wrote the manuscript, and managed the project.

806 **EXTENDED DATA: Crosstalk between AML and stromal cells triggers**
807 **acetate secretion through the metabolic rewiring of stromal cells**

808 Nuria Vilaplana-Lopera[1], Ruba Almaghrabi[1], Grigorios Papatzikas[1], Vincent Cuminetti[2], Mark Jeeves[1],
809 Elena González[1], Alan Cunningham[3], Ayşegül Erdem[3], Frank Schnuetgen[4,5,6], Manoj Raghavan[1,7],
810 Sandeep Potluri[1,7], Jean-Baptiste Cazier[1], Jan Jacob Schuringa[3], Michelle AC Reed[1], Lorena Arranz[2],
811 Ulrich L Günther[1,8*] and Paloma Garcia[1,9*],

812 [1] Institute of Cancer and Genomic Sciences, University of Birmingham, Birmingham B15 2TT, United Kingdom
813 [2] Stem Cell Ageing and Cancer Research Group, Department of Medical Biology, Faculty of Health Sciences, UiT – The Arctic
814 University of Norway, 9019 Tromsø, Norway
815 [3] Department of Experimental Hematology, University Medical Center Groningen, University of Groningen, Hanzeplein 1,
816 9700 RB, Groningen, The Netherlands.
817 [4] Department of Medicine, Hematology/Oncology, University Hospital Frankfurt, Goethe-University, 60590 Frankfurt,
818 Germany.
819 [5] Frankfurt Cancer Institute, Goethe-University Frankfurt, 60596 Frankfurt, Germany.
820 [6] German Cancer Consortium (DKTK), partner site Frankfurt/Mainz, and German Cancer Research Center (DKFZ),
821 Heidelberg, Germany
822 [7] Centre for Clinical Haematology, University Hospitals Birmingham NHS Foundation Trust, Queen Elizabeth Hospital,
823 Queen Elizabeth Medical Centre, Birmingham, United Kingdom.
824 [8] Institute of Chemistry and Metabolomics, University of Lübeck, 23562 Lübeck, Germany
825 [9] Corresponding author
826 [*] These two authors are co-senior authors.

827

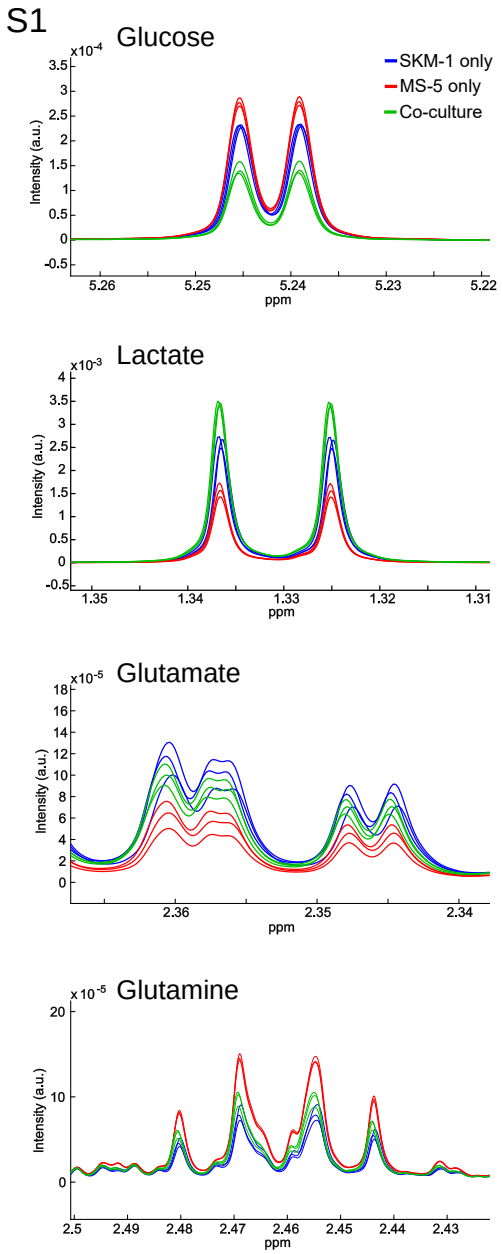

Extended Data Figure 1. Other extracellular metabolite levels in co-cultures with SKM-1 and MS-5 cells

Sections of ^{1}H-NMR spectra from extracellular medium samples of SKM-1 cells cultured alone (blue), MS-5 cells cultured alone (red) and SKM-1 and MS-5 cells in co-culture (green) after 24 hours of culture, corresponding to glucose, lactate, glutamate and glutamine.

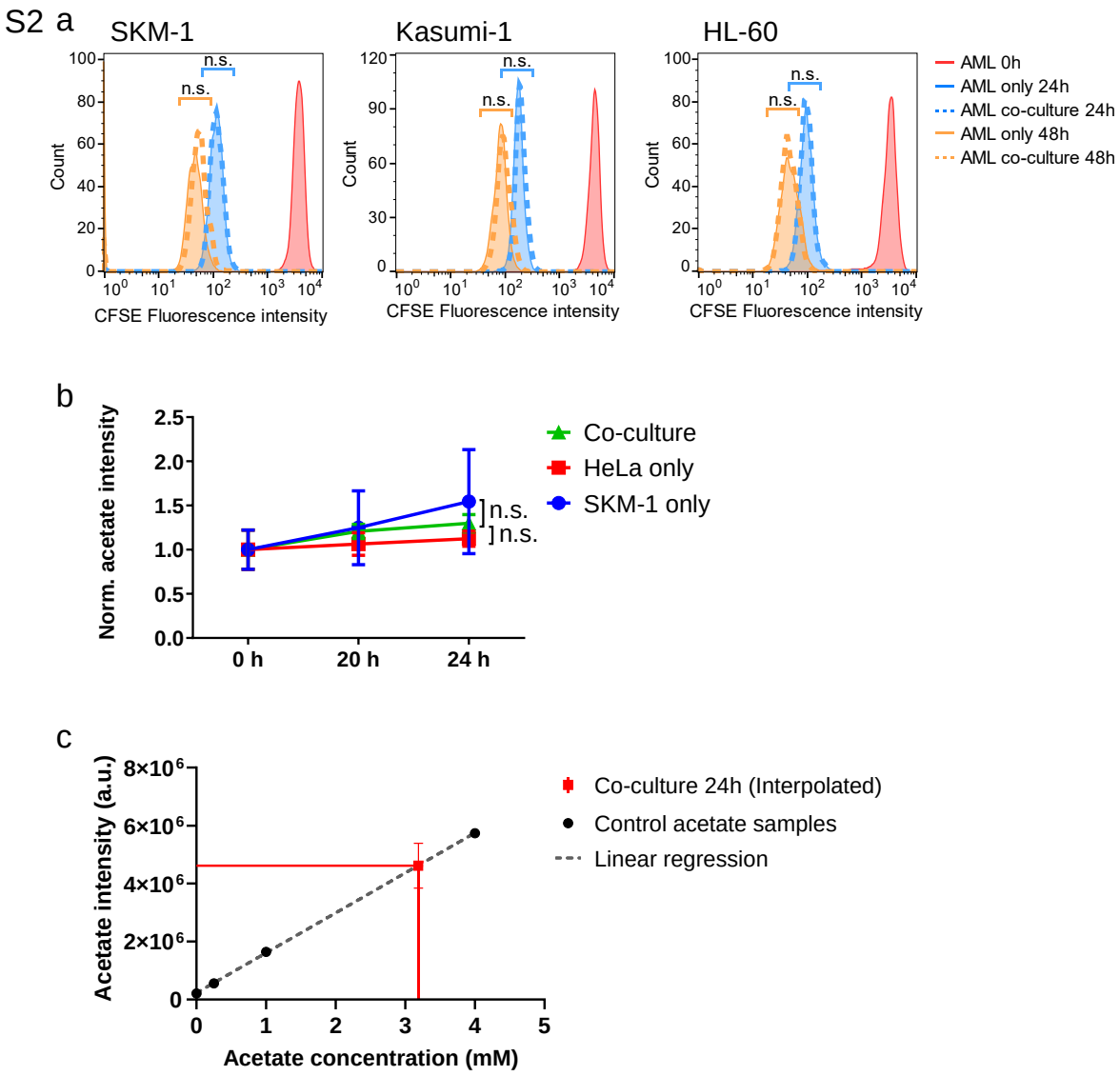

Extended Data Figure 2. Proliferation in co-culture, co-culturing AML cells with an unrelated cell line (HeLa) and titration of acetate concentration in co-culture

(**a**) CFSE cell proliferation analysis in AML cell lines alone or in co-culture with MS-5 cells. The population of living cells was gated, and 1500 cells for each condition were randomly selected and plotted. The geometric mean for each population and time point was compared between cells alone or in co-culture by performing an unpaired unpaired Student's t-test and p-values were represented as n.s. for not significant. Each histogram is representative of n=3 independent experiments. (**b**) Extracellular acetate levels in SKM-1 cells cultured alone (blue), HeLa cells cultured alone (red) and AML and HeLa cells in co-culture (green) at 0, 20 and 24 hours. Each point represents the mean of n=3 independent experiments and error bars represent standard deviation. An unpaired Student's t-test was applied for each condition (black brackets) and p-values are represented by n.s. for not significant. (**c**) Linear regression of acetate concentrations and detected intensities in ^{1}H-NMR

847 spectra (Intensity=$1.38 \cdot 10^6 \pm 1.6 \cdot 10^4$ x Acetate concentration + $2.27 \cdot 10^5 \pm 3.3 \cdot 10^4$; R^2=0.9987). The
848 intensities detected in samples of co-culture were interpolated to obtain the estimate acetate
849 concentration in co-culture (3.09 mM). Each point represents the mean of n=3 independent
850 experiments and error bars represent standard deviation.

851

S3

a

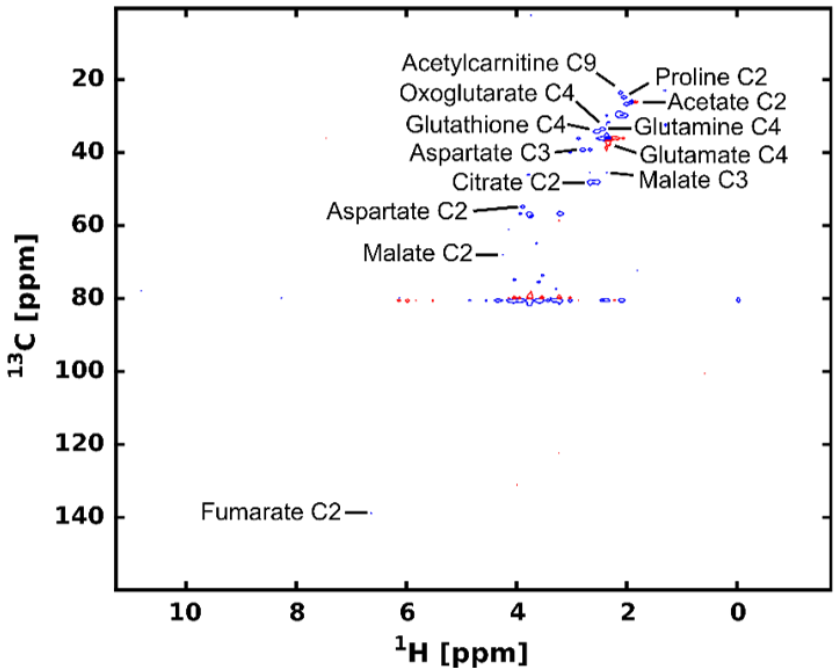

b

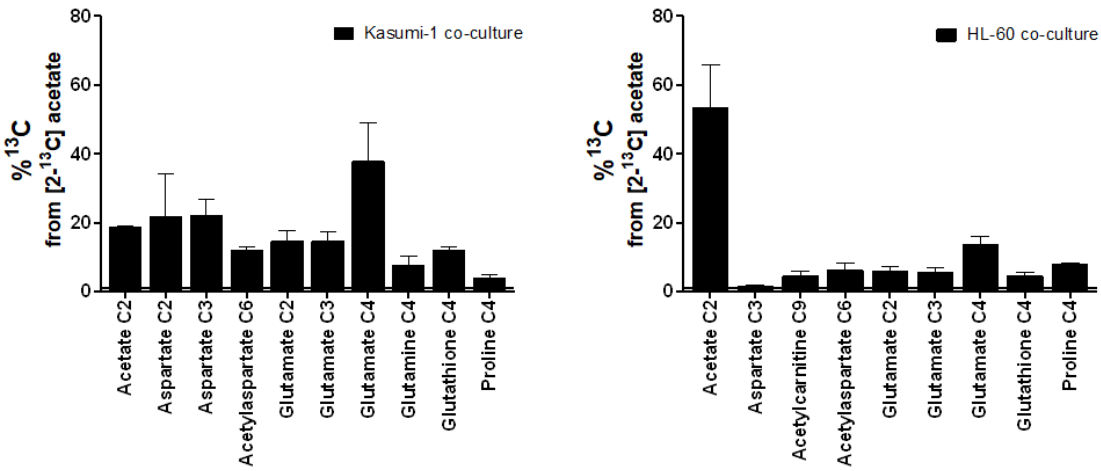

Extended Data Figure 3. Label incorporation from [2-^{13}C]acetate in SKM-1 and MS-5 cells cultured alone

(**a**) Example of metabolites assigned in a ^{1}H-^{13}C-HSQC spectrum from a polar extract from SKM-1 cells cultured with [2-^{13}C]acetate for 2 hours. ^{13}C percentages were calculated in 13 carbons from 11 different metabolites. The exact chemical shifts for each carbon are: acetate C2, 1.91 ppm (^{1}H) – 26.1 ppm (^{13}C); aspartate C2, 3.89 ppm (^{1}H) – 55.0 ppm (^{13}C); aspartate C3, 2.82 ppm (^{1}H) – 39.4 ppm (^{13}C); acetylcarnitine C9, 2.15 ppm (^{1}H) – 23.4 ppm (^{13}C); citrate C2, 2.52 ppm (^{1}H) – 48.2 ppm (^{13}C);

860 fumarate C2, 6.51 ppm (^{1}H) – 138.2 ppm (^{13}C); glutamate C4, 2.34 ppm (^{1}H) – 36.1 ppm (^{13}C);
861 glutamine C4, 2.44 ppm (^{1}H) –33.7 ppm (^{13}C); oxoglutarate C4, 2.43 ppm (^{1}H) – 33.4 ppm (^{13}C);
862 glutathione C4, 2.55 ppm (^{1}H) – 34.2 ppm (^{13}C); malate C2, 4.28 ppm (^{1}H) – 73.2 ppm (^{13}C); malate
863 C3, 2.68 ppm (^{1}H) – 45.4 ppm (^{13}C); and proline C4, 2 ppm (^{1}H) – 26.6 ppm (^{13}C). (**b**) ^{13}C percentages
864 on polar metabolites in Kasumi-1 and HL-60 cells in co-culture with MS-5 cells. Cells were co-
865 cultured for 24 hours before the addition of extra 4 mM sodium [2-^{13}C]acetate. Bars represent the
866 mean of the ^{13}C percentage and error bars represent the standard deviation of n=3 independent
867 experiments. ^{13}C natural abundance is represented as a black bar at %^{13}C = 1.1.

868

S4 a

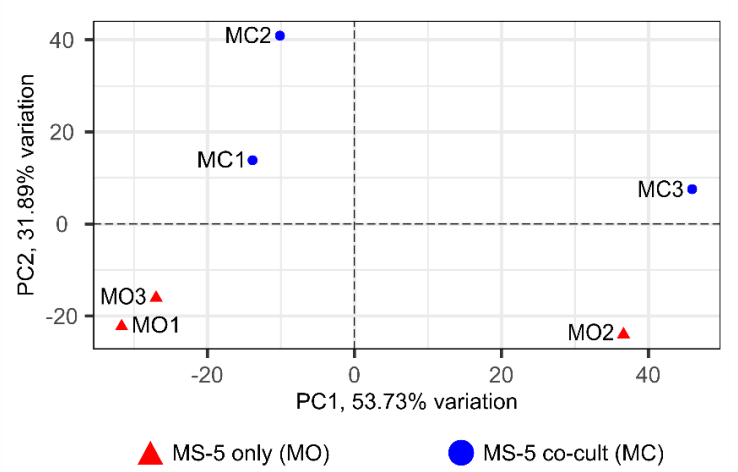
MC2
MC1
MC3
MO3
MO1
MO2
PC2, 31.89% variation
PC1, 53.73% variation
40
20
0
-20
-20
0
20
40
MS-5 only (MO)
MS-5 co-cult (MC)

b

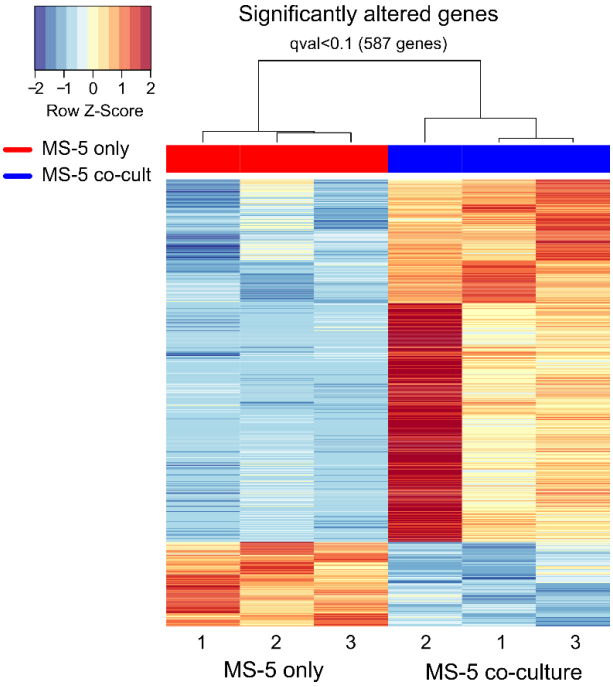
Significantly altered genes
qval<0.1 (587 genes)
−2 −1 0 1 2
Row Z-Score
MS-5 only
MS-5 co-cult
1 2 3 2 1 3
MS-5 only
MS-5 co-culture

c

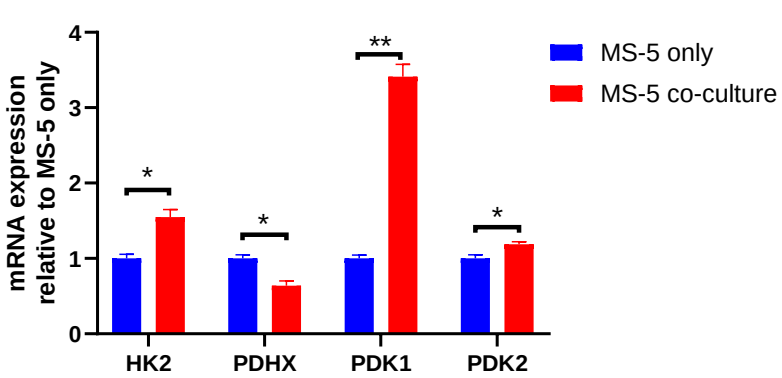
mRNA expression relative to MS-5 only
0
1
2
3
4
*
*
**
*
HK2
PDHX
PDK1
PDK2
MS-5 only
MS-5 co-culture

869

870 **Extended Data Figure 4. PCA component analysis, heat map of differentially expressed**
871 **genes and qPCR for MS-5 cells cultured alone and in co-culture with SKM-1 cells**

872 (**a**) PCA plot showing the clustering of individual samples of MS-5 cells cultured alone (MO) and MS-5
873 cells in co-culture (MC). The x and y axis values represent the variation between the sample groups.
874 Generated using Sleuth 0.30.0 R statistical package. **(b**) Heat map of differentially expressed genes in
875 MS-5 only (red) vs MS-5 co-culture (blue) calculated using the Wald statistical test, correcting for
876 multiple testing comparison employing the Benjamini-Hochberg method using a false discovery rate
877 threshold of 1% (q-value<0.01). Generated using Sleuth 0.30.0 R statistical package. **(c)** Quantitative
878 PCR mRNA expression values for RNA sequencing validation of MS-5 cells cultured alone and in co-
879 culture with SKM-1 cells. The gene set chosen was *Hk2*, *Pdhx*, *Pdk1* and *Pdk2*. mRNA quantification
880 was normalized to *B2m* house-keeping gene. Bars represent the mean and error bars represent the
881 SEM of three independent experiments. An unpaired Student's t-test was applied for each gene and
882 p-values are represented by * for p-value<0.05, ** for p-value<0.01 and *** for p-value<0.001.

883

S5

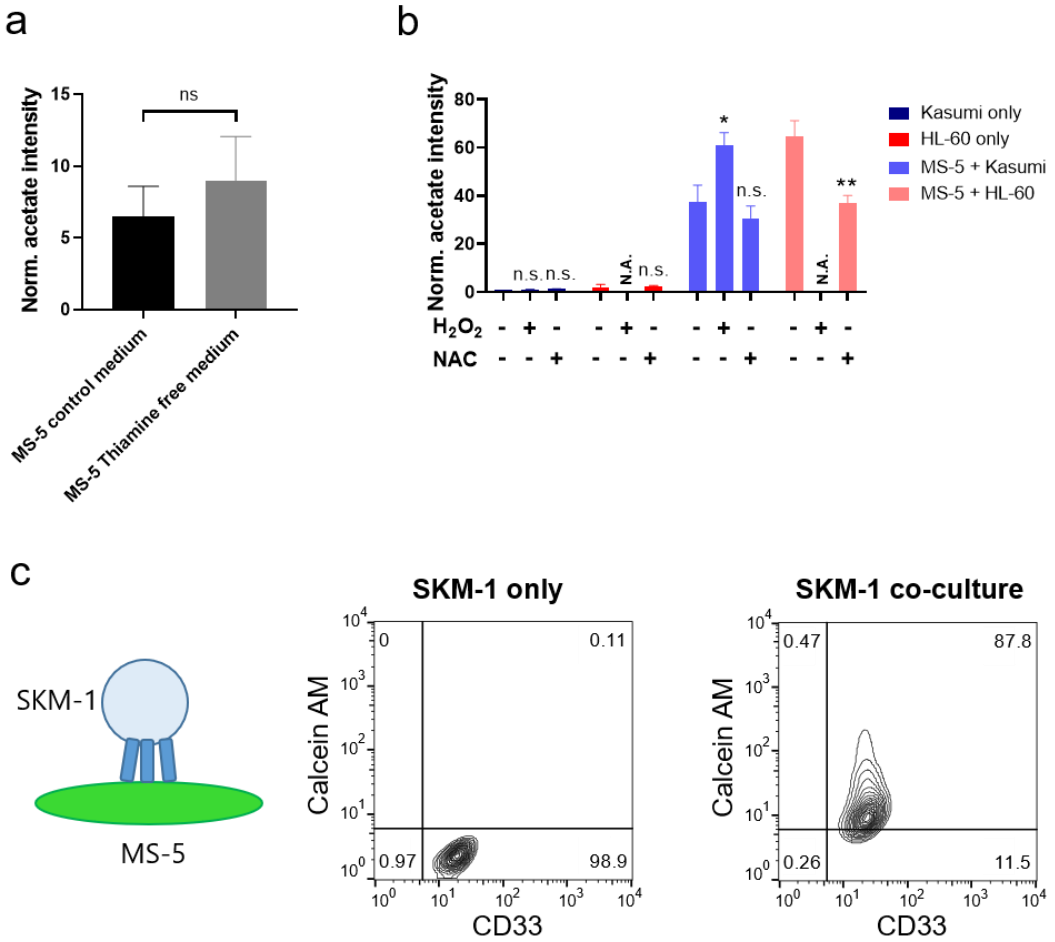

Extended Data Figure 5. Acetate secretion in thiamine free medium and after modulating ROS levels and calcein-AM transfer through GAP junctions in AML-stromal co-cultures

(**a**) Extracellular acetate levels in MS-5 cells cultured in control medium (black) or in thiamine-depleted medium (grey) after 24 hours. (**b**) Extracellular acetate levels in Kasumi (navy blue) and HL-60 (red) cultured alone and in co-culture (light blue and light red) for 24 hours in a control medium, medium with 50 µM H_2O_2 or medium with 5 mM NAC. Acetate levels for HL-60 cells cultured alone or under co-culture with 50 µM H_2O_2 are not shown as treatment 50 µM H_2O_2 severely impaired their viability. N.A. = not analysed. For **a** and **b** each point represents the mean of n=3 independent experiments and error bars represent standard deviation. An unpaired Student's t-test was applied for each condition (black brackets) and p-values are represented by n.s. for not significant. * for p-value<0.05 and ** for p-value<0.01. (**c**) Representative flow cytometry diagrams showing CD33 and calcein-AM green fluorescence in SKM-1 cells cultured alone or SKM-1 cells in co-culture with Calcein-AM-stained MS-5 cells after 3 hours. Frequencies of gated cell populations are indicated.

899 **Extended Data Table 1. Primary AML samples' additional information**

Samples obtained from Martini Hospital, UMCG

(used in figure 1e)

Patient	Tissue of origin	Type of AML (FAB)	Karyotype	Other mutations	Risk
AML1	PB	M5	Normal	FLT3-ITD; NPM1; DNMTA3; IDH2	Adv
AML2	PB	M1	Unknown	-	Adv

900

Samples obtained from University Hospital Birmingham NHS Foundation Trust, UoB

(used in figure 1e and 4c)

Patient	Tissue of origin	Type of disease	Karyotype	Other mutations
AML3	PB	Secondary AML from MDS	46,XY	TET2; SRSF2; RUNX1; CEBPA; ASXL1
AML4	PB	Secondary AML from MDS	46,XY	NPM1 neg FLT3 neg
AML5	PB	AML M1 (FAB)	46 XX	FLT3-ITD, 2xWT1, CEBPA
AML6	PB	AML M2 (FAB)	46 XX	-
AML7	PB	AML M4 (FAB)	46 XY	-

901

902